

**Modeling salami drying  
with different approaches  
and validation  
during industrial ripening**

**Giovanni Cascone**





Unione Europea



*Ministero dell'Istruzione,  
dell'Università e della Ricerca*



UNIVERSITÀ DEGLI  
STUDI DI SALERNO

**FONDO SOCIALE EUROPEO**  
**Programma Operativo Nazionale 2000/2006**  
**“Ricerca Scientifica, Sviluppo Tecnologico, Alta Formazione”**  
**Regioni dell’Obiettivo 1 – Misura III.4**  
**“Formazione superiore ed universitaria”**

*Department of Industrial Engineering*

*Ph.D. Course in Chemical Engineering  
(XVI Cycle-New Series, XXX Cycle)*

**MODELING SALAMI DRYING  
WITH DIFFERENT APPROACHES  
AND VALIDATION  
DURING INDUSTRIAL RIPENING**

**Supervisor**

*Prof. Michele Miccio*

**Ph.D. student**

*Giovanni Cascone*

**Ph.D. Course Coordinator**

*Prof. Ernesto Reverchon*



# Table of Contents

List of Figures .....	III
List of Tables.....	VII
List of Publications .....	IX
Journal papers.....	IX
Conference proceedings .....	IX
Abstract .....	XI
Introduction.....	1
1.1 Introduction to salami ripening .....	1
1.2 Ventilated industrial chambers.....	4
1.3 Ripening process description .....	6
1.4 The PON “SafeMeat” project.....	7
1.5 The COMSOL Multiphysics® software .....	9
Modeling of salami ripening using a homogeneous approach .....	11
2.1 Preface.....	11
2.2 Experimental activities.....	11
2.2.1 Dodaro ripening test.....	11
2.2.2 SSICA ripening test.....	17
2.3 Mathematical modeling.....	21
2.4 Comsol Multiphysics® code implementation.....	24
2.5 Simulation results.....	28
2.6 Comparison between predicted and experimental results .....	32
2.7 Conclusive remarks .....	39
Modeling of salami ripening using a heterogeneous approach .....	41
3.1 Preface.....	41
3.2 Experimental activities.....	42
3.3 Mathematical modeling.....	44
3.4 Comsol Multiphysics® code implementation.....	47
3.5 Simulation results.....	50
3.6 Comparison between predicted and experimental results .....	51
3.7 Conclusive remarks .....	53
Modeling of meat drying as a porous medium based on ad hoc experimental apparatus and procedure.....	55
4.1 Experimental .....	55
4.1.1 Apparatus .....	55
4.1.2 Procedure.....	58
4.1.3 Results .....	60
4.2 Mathematical modeling.....	67
4.3 Comsol Multiphysics® code implementation.....	67

---

4.3.1 Drying.....	68
4.3.2 Optimization procedure for diffusivity parameter estimation .....	69
4.4 Simulation results .....	72
4.5 Comparison between predicted and experimental results .....	73
4.5.1 Drying.....	73
4.5.2 Optimization procedure for diffusivity parameter estimation .....	74
4.6 Conclusive remarks .....	78
Conclusion and perspectives .....	79
Bibliography.....	81
APPENDIX A .....	85
Arduino programming.....	85

# List of Figures

Figure 1. Schematic representation of air circulation in an ascending-flow ripening chamber .....	4
Figure 2. Flow diagram of the processing of dry and semidry fermented sausages .....	7
Figure 3. The COMSOL Desktop with its major windows in a widescreen layout.....	9
Figure 4. Images of the same sausage sampled at ripening days 0, 2, 6, 13, 17, 24 (The radius of the fresh sausage is about $R_0=20$ mm) .....	13
Figure 5. Images of EVO sausages at the startup of the ripening test .....	18
Figure 6. Geometry of the mathematical model for mass balance and energy balance .....	22
Figure 7. Cylindrical 2D axi-symmetric geometry (A) and mesh (B).....	24
Figure 8. Image of a ready-to-eat Turista dry sausage (A) compared to various geometric representations: irregular 2D axi-symmetric (B) and its mesh (C), irregular 3D geometry (D) and its mesh (E)).....	26
Figure 9. Water concentration ( $\text{mol/m}^3$ ) profile as a function of the radial position ( $R$ ) parametrically in the ripening day. (Dodaro test 2015: Simulation in axis-cylindrical geometry with moving mesh).....	29
Figure 10. 3D plot of the water concentration ( $\text{mol/m}^3$ ) in the sausage at day 1 (A), at day 24 (B) and at day 24 with zoom on the edge (C) (Dodaro test 2015: Simulation in 2D axi-cylindrical geometry with moving mesh).....	30
Figure 11. Zoom of mesh decrease in 2D domain from day 1 (A) to day 24 (B) during simulation of sausage ripening (Dodaro test 2015) .....	30
Figure 12. Temperature ( $K$ ) profile as a function of the radial position ( $R$ ) parametrically in the ripening day. (Dodaro test 2015: Simulation in 2D axi-cylindrical geometry with moving mesh) .....	31
Figure 13. 3D plot of the temperature ( $K$ ) in the sausage at day 1(A) and at day 24 (B) (Dodaro test 2015: Simulation in 2D axi-cylindrical geometry with moving mesh) .....	31
Figure 14. 3D color maps representing the predicted water concentration at the very end of Turista salami ripening in A) cylindrical 2D axi-symmetric geometry, B) irregular 2D axi-symmetric geometry, C) irregular 3D geometry, D) cylindrical 2D axi-symmetric geometry with shrinking .....	32
Figure 15. Experimental and simulated weight loss for cylindrical 2D axi-symmetric geometry (Turista Buonpiemonte reference sausage) .....	33
Figure 16. Experimental and simulated weight loss for irregular 2D axi-symmetric geometry (Turista Buonpiemonte reference sausage) .....	33

---

Figure 17. <i>Experimental and simulated weight loss for irregular 3D geometry (Turista Buonpiemonte reference sausage)</i> .....	34
Figure 18. <i>Experimental and simulated weight loss for cylindrical 2D axis-symmetric geometry with shrinking (Turista Buonpiemonte reference sausage)</i> .....	34
Figure 19. <i>Comparison between experimental and predicted sausage weight loss in cylindrical 2D axis-symmetric geometry. Dodaro test 2015: model predictions a) without shrinking; b) with shrinking (I: set of experimental data for mold Inoculated sausages; NI: set of experimental data for Non-Inoculated sausages)</i> .....	36
Figure 20. <i>Comparison between experimental and predicted sausage water content in cylindrical 2D axis-symmetric geometry. Dodaro test 2015: model predictions a) without shrinking; b) with shrinking (I: set of experimental data for mold Inoculated sausages; NI: set of experimental data for Non-Inoculated sausages)</i> .....	37
Figure 21. <i>Comparison between experimental and predicted diameter shrinkage curves in cylindrical 2D axis-symmetric geometry. Dodaro test 2015: model predictions without shrinking (dashed line) and with shrinking (solid line) (I: set of experimental data for mold Inoculated sausages; NI: set of experimental data for Non-Inoculated sausages)</i> .....	38
Figure 22. <i>Comparison between experimental and predicted sausage weight loss in cylindrical 2D axis-symmetric geometry. SSICA test No. 3 with prediction of shrinking for a) Traditional sausage; b) EVO sausage</i> .....	39
Figure 23. <i>Comparison between experimental and predicted sausage weight loss in cylindrical 2D axis-symmetric geometry. SSICA test No. 4 with prediction of shrinking for a) Traditional sausage; b) EVO sausage</i> .....	39
Figure 24. <i>The muscle split into components with fibers and the locations of muscle water compartments (Pearce, 2011)</i> .....	41
Figure 25. <i>Schematic illustration of a hexagonal system as an approximation of the fiber structure of meat (Da-Wen Sun et al., 2002)</i> .....	42
Figure 26. <i>Pictures of meat samples cut as cubes of about 10 mm side: A) Fresh cut, B) Frozen, A) Freeze-dried</i> .....	43
Figure 27. <i>SEM freeze-died samples in 20 <math>\mu\text{m}</math> scale (A) and in 200 <math>\mu\text{m}</math> scale (B)</i> .....	43
Figure 28. <i>Schematic showing the various porous media formulations and their interrelations in the context of food processes (Datta, 2007)</i> .....	44
Figure 29. <i>Prevailing mechanisms of water transport in porous food materials. A, liquid diffusion and capillary flow; B, vapor diffusion; C, desorption of sorbed water (Saravacos, 2001)</i> .....	45
Figure 30. <i>Schematic representation of the water flow path in the minced mix in radial direction (from left to right). The meat beads (parallel line pattern) and the fat beads (solid fill) have the same size (<math>d = 5\text{ mm}</math>)</i> .....	47
Figure 31. <i>Cylindrical 2D axis-symmetric mesh (A) and its zoom (B) in heterogeneous domain</i> .....	48

---

Figure 32. Water concentration ( $\text{mol/m}^3$ ) profile as a function of the radial position ( $R$ ) (A) and the axial position ( $H$ ) (B) parametrically in the ripening day.....	50
Figure 33. The most significant water concentration profiles during the ripening time .....	51
Figure 34. Zoom of plot of the water concentration ( $\text{mol/m}^3$ ) in the sausage at day 1 in 2D (A) and 3D (B) view and at the day 24 in 2D (C) and 3D (D) view .....	51
Figure 35. Comparison between experimental and predicted sausage weight loss in heterogeneous (porous medium) and homogeneous model .....	52
Figure 36. Comparison between experimental and predicted values of the average sausage water content in heterogeneous (porous medium) and homogeneous model .....	52
Figure 37. Comparison between experimental and predicted diameter shrinkage curves: simulation with the homogeneous model with shrinking and calculation of a diameter reduction with the data of the porous medium....	53
Figure 38. Experimental apparatus with the sample holder and the various sensors.....	56
Figure 39. Arduino nano picture (A) and pin input-output configuration (B) .....	56
Figure 40. Picture of DHT22 sensor (A), HX711 load cell (B), moisture sensor (C) .....	57
Figure 41. PLX-DAQ pop-up image.....	58
Figure 42. Meat sample holder picture .....	58
Figure 43. Specimen 3D geometry (A) and Mesh (B).....	68
Figure 44. Water concentration ( $\text{mol/m}^3$ ) profile through the length of the sample $L$ (m) parametrically in the drying day for test A (A) and test B (B)	72
Figure 45. 3D plot of the water concentration ( $\text{mol/m}^3$ ) in the sample at day 3 for test A (A) and test B (B) .....	72
Figure 46. Comparison between experimental and predicted weight loss for one exchange surface experiment .....	73
Figure 47. Comparison between experimental and predicted weight loss for two exchange surfaces experiment .....	73
Figure 48. Comparison between experimental and predicted moisture concentration profile for one exchange surface experiment (A) and two exchange surfaces experiment (B).....	74
Figure 49. Effective diffusivity simulation and experimental weight loss comparison for one surface experiment .....	75
Figure 50. Effective diffusivity simulation and experimental concentration profile comparison @ $t=48$ h for 1 surface experiment.....	76
Figure 51. Effective diffusivity simulation and experimental weight loss comparison for two exchange surfaces experiment .....	76
Figure 52. Capillary diffusivity simulation and experimental weight loss comparison for one surface experiment .....	77

---

Figure 53. <i>Capillary diffusivity simulation and experimental concentration profile comparison @<math>t=48</math> h for one surface experiment .....</i>	77
Figure 54. <i>Capillary diffusivity simulation and experimental weight loss comparison for two surface experiment .....</i>	78

# List of Tables

Table 1. <i>Classification of fermented sausages</i> .....	2
Table 2. <i>Dodaro recipe of a typical "non-spicy sausage" of the Calabria region</i> .....	12
Table 3. <i>Ripening program (set points of temperature and relative humidity) of the industrial ripening chamber at the Dodaro SpA factory throughout the test conducted on a lot of 300 kg of a typical "non-spicy sausage"</i> .....	12
Table 4. <i>Weight (g) of single inoculated and non-inoculated sausage at different levels during the Dodaro ripening test</i> .....	14
Table 5. <i>Circumference (mm) of single inoculated and non-inoculated sausage at different levels during the Dodaro ripening test</i> .....	15
Table 6. <i>% weight loss (WL) and % diameter reduction (DR, from <math>D_0=40</math> mm) of single inoculated and non-inoculated sausage during the Dodaro ripening test</i> .....	16
Table 7. <i>% moisture content of single inoculated and non-inoculated sausage at different height levels during the Dodaro ripening test</i> .....	17
Table 8. <i>Recipe of "EVO sausage"</i> .....	18
Table 9. <i>Weight (g) of rack sticks at different levels for the SSICA test No. 3 (each stick carries 10 sausages of either EVO or traditional type)</i> .....	19
Table 10. <i>% weight loss for an average single sausage in the SSICA test No. 3 on EVO (initial mass 523.2 g) and traditional (initial mass 522.7 g) sausages</i> .....	20
Table 11. <i>Weight (g) of rack sticks at different levels for the SSICA test No. 4 (each stick carries 10 sausages of either EVO or traditional type)</i> .....	20
Table 12. <i>% weight loss for an average single sausage in the SSICA test No. 4 on EVO (initial mass 483.8 g) and traditional (initial mass 504.0 g) sausages</i> .....	21
Table 13. <i>Code data input for Turista salami ripening</i> .....	25
Table 14. <i>Code data input for the Dodaro sausage ripening</i> .....	27
Table 15. <i>Code data input for EVO and traditional sausage ripening (SSICA tests No. 3 and 4)</i> .....	28
Table 16. <i>Code data input with porous media model for the Dodaro sausage ripening</i> .....	49
Table 17. <i>Diffusivity parameters of the potato from literature</i> .....	49
Table 18. <i>Experimental data for 1 free surface samples (A) and 2 free surfaces samples (B)</i> .....	60
Table 19. <i>Weight loss data log for the triplicated experiment with 1 exchange surface (A)</i> .....	61

---

Table 20. <i>Weight loss data log for the triplicated experiment with 2 exchange surface (B)</i> .....	63
Table 21. <i>C/C<sub>0</sub> data log for triplicated 1-moisture exchange surface experiment (A)</i> .....	65
Table 22. <i>C/C<sub>0</sub> data log for triplicated 2-moisture exchange surface experiment (B)</i> .....	66
Table 23. <i>Code data input with porous media model for the experimental drying conditions</i> .....	69
Table 24. <i>Code data input with porous media model for the 1D experimental drying case</i> .....	71
Table 25. <i>Starting parameters in optimization of effective diffusivity</i> .....	71
Table 26. <i>Starting parameters in optimization of capillary diffusivity</i> .....	71
Table 27. <i>Effective diffusivity parameters as optimization result</i> .....	75
Table 28. <i>Capillary diffusivity parameters as optimization result</i> .....	76

# List of Publications

## Journal papers

Cascone Giovanni, Miccio Michele, Setegn Hulegezie Getnet, Diaferia Carlo (2015). A tool for modeling and simulation of irregular shape and shrinking salami during drying. In: Chemical Engineering Transactions. vol. 43, p. 103-108, ISBN: 978-88-95608-34-1, DOI:10.3303/CET1543018.

Cascone Giovanni, Miccio Michele, Dodaro Massimiliano, Longo Franco, Seta Lucia (2017). Modeling and Simulation of Fermented Sausages Ripening with a Heterogeneous Porous Media Approach. In: Chemical Engineering Transactions. vol. 57, p. 2029-2034, ISBN: 978-88-95608-48-8, DOI: 10.3303/CET1757339.

Miccio Michele, Fraganza Michela, Cascone Giovanni, Diaferia Carlo, Ferrara Massimo, Magistà Donato, Perrone Giancarlo, Dodaro Massimiliano, Longo Franco, Seta Lucia (2017). On Measuring, Modelling and Validating Growth of Surface Molds through Image Analysis in Industrial Salami Ripening. In: Chemical Engineering Transactions. vol. 57, p. 2011-2016, ISBN: 978-88-95608-48-8, DOI: 10.3303/CET1757336.

Cascone Giovanni, Sofia Daniele, Miccio Michele, Poletto Massimo (2017). Analysis and modeling of meat drying process using a porous media approach. Submitted in December 2017 to Journal of Food Engineering.

## Conference proceedings

Cascone Giovanni, Miccio Michele, Seta Lucia, Longo Franco, Dodaro Massimiliano (2015). Modeling and Simulation of Relevant Changes in Fermented Sausages during Ripening. In: Recent Advances in Fluid Mechanics and Thermal Engineering. p. 106-113, WSEAS Press, ISBN: 978-1-61804-311-5, Salerno, Italy, June 27-29, 2015.

Cascone Giovanni, Miccio Michele, Diaferia Carlo, Dodaro Massimiliano, Fraganza Michela, Longo Franco, Seta Lucia (2016). Modello matematico di ottimizzazione della stagionatura di un batch industriale di salami. In proceedings of GRICU Meeting "Gli orizzonti 2020 dell'Ingegneria Chimica", September 12-14, 2016. Anacapri (NA), Italy.

---

Miccio Michele, Fraganza Michela, Cascone Giovanni, Diaferia Carlo, Dodaro Massimiliano, Longo Franco, Seta Lucia, Ferrara Massimo, Magistà Donato, Perrone Giancarlo (2016). Misura e modellazione della crescita nel tempo di muffe superficiali su salami attraverso tecniche di analisi d'immagine, In proceedings of GRICU Meeting "Gli orizzonti 2020 dell'Ingegneria Chimica", September 12-14, 2016. Anacapri (NA), Italy.

Cascone Giovanni, Carlo Diaferia, Raffaella Ferraioli, Michela Fraganza, Michele Miccio (2017). Data Analysis in a Batch Salami Ripening Chamber for Real-Time Process Monitoring and Control. In proceedings of 6th ACEC, ISBN: 978-1-63248-138-2, 09-10 December, 2017, Rome, Italy.

Cascone Giovanni, Michele Miccio, Carlo Diaferia, Massimiliano Dodaro, Michela Fraganza, Franco Longo, Lucia Seta (2017). Cost Optimization in Batch Industrial Salami Ripening through Mathematical Modeling. In proceedings of 6th ACSEE, ISBN: 978-1-63248-139-9, 09-10 December 2017, Rome, Italy.

# Abstract

Nowadays, ripening of salami under natural conditions has been replaced by batch production in ventilated industrial chambers. Hence, the same product quality can be obtained regardless of local, environmental and climatic conditions. Nevertheless, carefully designed and monitored process conditions are necessary to achieve the targeted weight loss and quality of dry fermented sausages. Therefore, the availability of reliable mathematical models and manageable software codes for sausage drying, maturation and optimal production are highly welcome.

This thesis deals with the development and the progressive improvement of a mathematical model (and its underlying software solving code) of sausage drying during actual industrial ripening conditions. The mathematical model considered as the start point had the following features: 1D, axi-symmetric, time-invariant cylindrical geometry; homogeneous and isotropic material; no distinction between the inner part (core) and the casing; water concentration as a distributed parameter; the internal water transfer rate as a concentration-dependent Fickian diffusion with the assumption of an effective diffusion coefficient depending on the local water content. Starting from this, different and more realistic improvements of the sausage geometrical representation have been pursued: cylindrical 2D axi-symmetric geometry, irregular 2D axi-symmetric geometry, irregular 3D geometry, cylindrical 2D axi-symmetric geometry with volume shrinking. From the comparison of the various model predictions with the experimental data that originated from external industrial-scale ripening tests, it was possible to deduce that a more realistic irregular geometry is influential on the computational load, but irrelevant to the prediction of the sausage weight loss, i.e., the most well-known process performance variable. For this reason, a simple cylindrical shape could be used to implement a more realistic variable-volume simulation model. Another assessment that was made with this study was that the ripening process can be considered isothermal because the temperature transients, e.g., occurring at startup or after a temperature set point change, have a characteristic time that is negligible when compared to that characteristic of mass transfer. A natural, but necessary development of the work has been a mathematical model of fermented sausage drying relying on an innovative description of the sausage as a heterogeneous material, i.e., separately made of lean meat and fat, and a porous medium. The fat is considered as an inert matter dispersed in the meat matrix, while the lean meat is considered as a porous medium in which the transport phenomena of water take place to the outside of the matrix during the ripening process. Porosimetry and image

---

analysis were applied to the meat matrix to demonstrate the goodness of the porous media approach. However, the direct implementation of the above porous media approach in a calculation code has been prevented by the lack of correlations for the water diffusion in the porous meat matrix. For this reason, an experimental setup was thought that would allow an evaluation of the dependence of the diffusivity from the local water content in the meat matrix during the drying process. The experimental apparatus allows real-time monitoring of the sample weight and water concentration profiles that are established in the material under investigation. The sample is kept in a constant-humidity, controlled atmosphere during the whole experiment. By coupling the model simulation with porous media approach and the experimental data from such an apparatus, it is possible to simulate the drying process of a particular material for which the internal water diffusion characteristics are unavailable or unrealistic in the literature. In particular, two correlations for the water diffusion in the porous meat matrix (e.g.,  $D = f(\text{local moisture content, Temperature})$ ) were found in literature, but their application or validation to the case of meat-based food was missing. So, it was possible to determine optimal parameters for them, just tailored for the lean meat under investigation here. Therefore, with a more reliable correlation for water diffusion and the calculation code based on the porous media approach, the prediction of the drying mechanism turned out more realistic and provided added value to the knowledge of the salami curing processes.

# Introduction

## 1.1 Introduction to salami ripening

Salami are cured traditional foods in different geographical parts of the world. In meat processing and within the fermented meat products, salami products are of major importance from historical, nutritional, and economic viewpoints (Zeuthen, 2007); early salami-type sausages were first produced in Italy at the time of the Roman empire (Zeuthen, 2007). A different denomination adopted for dry fermented sausages, often related to the local tradition or to the production area, is frequently matched by an actual diversity in products as far as: i) composition (e.g., type of meat, cut size of lean and fat, ingredients and additives, nature of the casing, microbial starters); ii) process and technique for drying and curing (e.g., long-maturing salami, short-maturing salami), as discussed by Zambonelli et al. (1992) and Toldrá et al. (2014). International examples of minced fermented meat products include salami, chorizo, pepperoni and saucisson (Toldrá et al., 2014).

Table 1 shows a general classification of the fermented sausage features with their features and ripening times (Lücke, 1994).

The preparation of salami is based on an apparently simple procedure. Once a prefixed recipe has been established or adopted, the salami production usually includes the following steps: 1) sorting and trimming of meat (it consists in the choice of the most suitable cuts, usually from pork, for the sausage preparation); 2) mincing and mixing (lean and fat cuts are ground at a low temperature; then salt, spices, additives, microbial starters and other ingredients are added); 3) filling a natural or synthetic gut with the above mixture; 4) fermentation and drying (sausages are moderately heated in a temperature range of 18-22 °C and in a range of relative humidity RH=50-75% for a period of 5-7 days); 5) ripening (sausages are further dried at a milder rate and led to complete maturation at a temperature of about 12°C and in a range of relative humidity RH=55-85% for a period depending on the product, from a few weeks to 2 months).

In modern times, salami have been extensively studied in the areas of food science and technology (Katz and Stinsky, 1987; Toldrá et al., 2014). The largely prevailing process in the salami production from fresh sausages is dehydration. The final product weight loss is high enough, generally about 1/3 of the initial weight, 20% of which is in the first processing week (Diaferia et al., 2011). The shelf life of fermented sausages belonging to the Italian tradition is determined by lowering free water (water activity, aw) below the limit for growth of spoilage microorganisms (Leistner, 1987). Water activity

reduction by drying and salt addition imparts stability to all kinds of meat (De Rosa et al., 2005; Toldrá et al., 2014), whereas fermentation mostly determines the characteristic texture and flavor (Zeuthen, 2008).

**Table 1.** *Classification of fermented sausages*

Category	Ripening times	Final water activity	Application of smoke	Examples
Dry, mould-ripened	> 4 weeks	< 0.90	No	Genuine italian salami French “saucisson sec”
Dry, mould ripened	> 4 weeks	< 0.90	Yes, (during fermentation)	Genuine Hungarian salami
Dry, no mould growth	> 4 weeks	< 0.90	Yes or not	German “Dauerwurst”
Semi-dry, mould-ripened	< 4 weeks	0.90 - 0.95	No	Various French and Spanish raw sausages
Semi-dry, no mould growth	< 4 weeks (usually 10 - 20 days)	0.90 - 0.95	Yes (with exceptions)	Most fermented sausages in Germany, The Netherlands, Scandinavia, USA etc.
Undried, spread-able	2 days to 2 weeks	0.94 - 0.97	Yes or not	German “Streichmettwurst”, Spanish “sobrasada”

The acquisition of scientific knowledge about the mechanisms involved in the maturation of the meats is fairly recent (Letablier et al., 1994; Pirone et al., 2007). Presently, the ability to describe the drying process depends on the knowledge of phenomena related, to a greater extent, to water transport inside the product and, to a lesser extent, to moisture evaporation from the outside surface. Of course, a gradient concentration of water between the inner part of the solid and its external surface establishes. Owing to salami granular structure, water actually moves in a complex way and the main transfer mechanisms are usually considered: i) capillary flow of free water; ii) bound water movement; iii) diffusion in liquid phase; iv) condensation-evaporation (Rossen et al., 1977- Okos et al., 1992). These mechanisms are often competitive (Baldini et al., 2001) and the drying kinetics is the consequence of their relative importance and interaction as well as the applied external conditions (Bessadok Jemai, 2013). The extrinsic variables controlling first drying and then ripening of fermented sausages are temperature, humidity and velocity of curing air (Baldini et al., 2001; Grau et al., 2014).

The local environmental conditions in traditional farm-based salami production (i.e., temperature, humidity and renewal rate of air) and the plant operating variables during the industrial ripening (i.e., temperature, humidity, velocity of curing air as well as the ventilation pattern) have always allowed the surface growth of a fungal population (Baldini et al., 2006), commonly composed of the *Penicillium* and *Aspergillus* species. These latter play an important role on the final quality of products, especially in industrial ripening.

The use of fungal inoculation during meat processing is a known practice (Spotti et al., 2008). When performed on fresh salami, the superficial fungal inoculum introduces an additional value (e.g., attractive surface appearance, easy detachment of the casing, etc.), and also works as a protective measure against growth of competitive molds able to produce even mycotoxins (Ferrara et al., 2016a; Magistà et al., 2016). Several studies have been made on surface molds from microbiological and toxigenic viewpoints (Ferrara et al., 2016b).

Either the surface growth or the differentiation of the fungal population do not appreciably affect the finally targeted weight loss for a commercial salami (Baldini et al., 2006), whereas the mass and energy transport phenomena at the sausage surface may be affected throughout the ripening time (Imre and Kornyei, 1990; Diaferia et al., 2011).

Mathematical modeling and simulation work has already been carried out in recent years and well addressed in literature as far as drying, fermentation and ripening of salami-type products. It is commonly assumed that dry sausages have a perfect cylindrical shape, their weight loss is due to water evaporation only and biochemical changes due to fermentation have no influence on weight loss (Imre and Kornyei, 1990). Fermented sausages have been usually modeled as a homogeneous and isotropic objects; water concentration is intended to be a “distributed parameter” variable. Imre and Kornyei (1990) subdivided salami structure into two parts, the inner paste (core) and the casing, having different chemical-physical and transport properties, and wrote different mass balance equations, respectively. Diaferia et al. (2011) considered 1D, axi-symmetric, homogeneous and time-fixed cylindrical geometry, then developed and validated a mathematical model predicting drying and temperature history of a single sausage, under both natural and forced air circulation. Fabbri and coworkers (Fabbri et al., 2011; Cevoli et al., 2014) introduced numerical modeling based on the methodology of finite elements in tackling the problem of salami drying and ripening. Cevoli et al. (2014) developed two parametric numerical models to study the moisture diffusion physics, during either salami ripening or the following storage in a closed packaging, taking account of the vapour exchange phenomena at the surface. Fabbri and Cevoli (2015) worked on a salami slice and discussed two finite element models of water diffusion taking account of the vapor exchange phenomena at the outer surface. One model was based on

the real fat and meat distribution in the slice, as acquired by image analysis, while a second, simpler one considered the salami material as homogeneous and imposed an equivalent value of diffusion coefficient, based on compositional equations (parallel, series, Maxwell and Krisher) or literature data.

Optimization with mathematical models of modern industrial salami ripening production is not very much treated in scientific literature. Tradition and rules of thumb hold, whereas many actions and decisions are taken by process technologist on the basis of his personal experience and historical data log. Imre and Kornyei (1990) elaborated a dynamic drying algorithm for salami and set up an automatic ripening control strategy. Bertolini et al. (2006), based on previous modeling works for the fluid-dynamic and thermal simulation of the above SSICA pilot cell (Grassi and Montanari, 2005), simulated and validated the batch ripening process for different salami. In addition, from the analysis of the low-period oscillation of the air flow into the cell, they found a particular configuration that optimizes the batch from the viewpoint of uniformity in the weight loss of individual sausages.

## 1.2 Ventilated industrial chambers

Nowadays, ripening of salami under natural conditions has been replaced by batch production in ventilated industrial chambers (Figure 1).

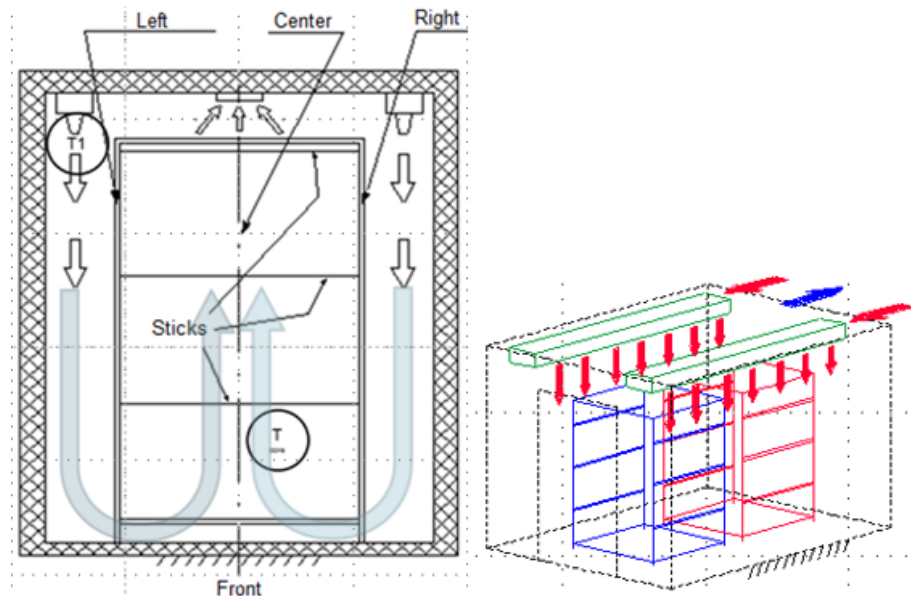


**Figure 1.** Schematic representation of air circulation in an ascending-flow ripening chamber

Hence, the same product quality can be obtained regardless of local, environmental (Kottke et al., 1996), and climatic conditions (Katz et al., 1987).

The most popular chamber used in industrial processes is the ascending flow ripening chamber. In this type of chamber, the inlet airflow is rationed between two main distribution ducts, which feed two inlet nozzle banks located at the outermost sides of the cell.

Thanks to this technology, the inlet airflow is rationed by a rotary distribution valve between two main distribution ducts, which feed two inlet nozzle banks located at the outermost sides of the cell ceiling. The inlet air flows are directed downward along the cell walls and merge over the cell floor, in a position that depends on the respective kinetic energy, therefore on the ratio between the two inlet air flow rates. The more unbalanced the inlet air flow rates, the wider the shifting of the air flows merging point from the cell midsection (Grassi and Montanari, 2005). Next, the air stream moves upwards toward an exhaust nozzle battery in the midsection of the cell ceiling. In this upward motion the air stream cyclically “bathes” the products hung on racks and placed in the central part of the cell, at the same time moisture and heat exchange occurs with the sausages under ripening.

In the industrial ascending flow ripening chambers, products are hung on racks and placed in the central part of the cell, so that a direct contact with the high velocity dry descending air streams is prevented.

This solution has been conceived in order to avoid placing air-feeding devices on the bottom of the cell; nevertheless the latter design solution would allow a direct ascending flow from the floor to the cell ceiling. The cell floor is subject to fouling due to the sausage dribble; therefore, devices placed on the cell bottom could be hard to clean, therefore constituting a source of potential pollutants. Moreover, these devices could be easily damaged during loading/unloading operations.

In an industrial chamber, therefore, carefully designed and monitored process conditions are necessary to achieve the targeted weight loss and several microbiological, physic-chemical and biochemical changes to guarantee the sensory quality of dry fermented sausages, as well as their chemical and microbial stabilization (Costa-Corredor et al., 2010; Toldrá et al., 2014).

### 1.3 Ripening process description

The whole sausage ripening process consists of a sequence of phases, as the following (Zambonelli et al., 1992):

- **1<sup>st</sup> phase: stabilization** of the introduced product. Chamber temperature: 5-7°C. It is aimed at obtaining a uniform product temperature, before start-up of the drying process. This phase is used only if the product loading time in the chamber is high and so it is necessary to avoid initial temperature differences.
- **2<sup>nd</sup> phase: low temperature drying** at 7-8 °C. This phase allows a weight loss of 2% in 12-20 hours and guarantees drying of the casing, which are very moistened because just washed. Only a few producers are equipped and actually adopt this phase.
- **3<sup>rd</sup> phase: heating**. In this phase the product attains a core temperature of about 18-20°C; the duration of the heating stage is a function of the chamber temperature, the sausage size and shape and the meat quality. A small weight loss is allowed by controlling the chamber relative humidity (RH). In this phase, temperature and a high humidity facilitate the sausage typical fermentation, which will give the distinctive taste and characteristic flavor.
- **4<sup>th</sup> phase: actual drying**. A strong dehydration and a drop in the chamber temperature characterize this phase, which results in the end of the above said fermentation. Beginning temperature: 18-22°C, RH: 50-75%.
- **5<sup>th</sup> phase: ripening**. This phase is a drying phase too, but at a milder rate. The chamber temperature decreases from an initial value of 17°C down to 12-13°C; RH is about 55-85%.

Fully automated operation of the ripening chamber ensures uniform circulation of curing air within the volume occupied by sausages inside the chamber.

The Figure 2 pictorially illustrates the above description (Toldrá, 2010).

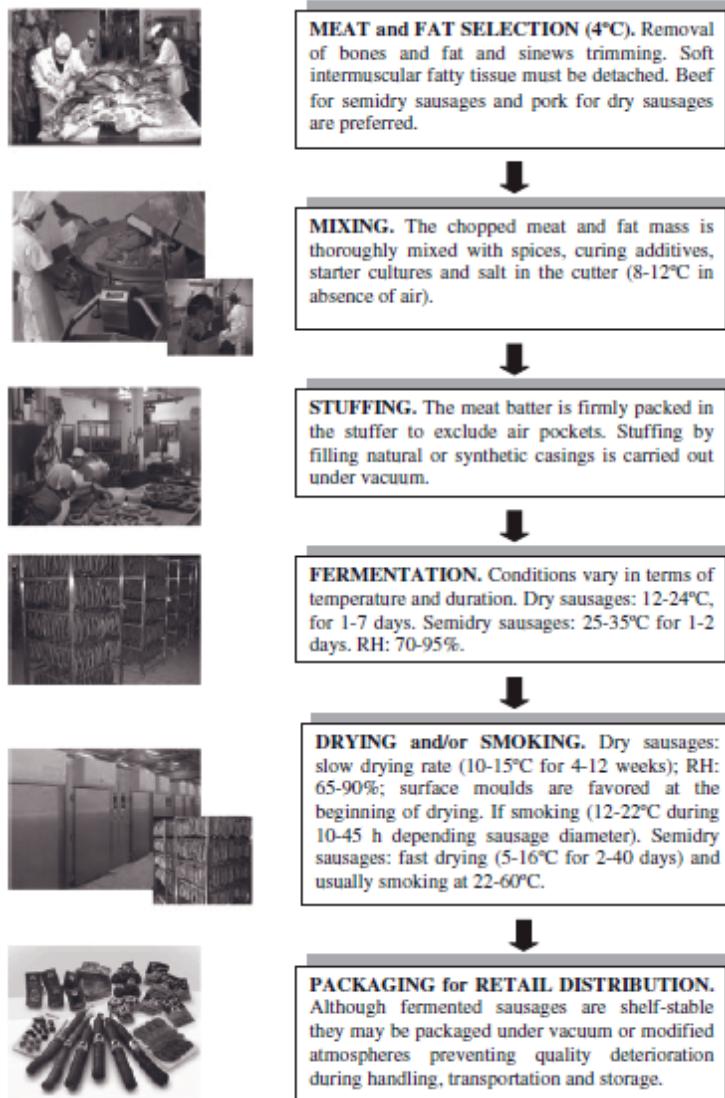


**Figure 2.** Flow diagram of the processing of dry and semidry fermented sausages

#### 1.4 The PON “SafeMeat” project

The motivation for the present thesis, the support for many of the activities and a consistent amount of experimental data come from the research project PON01\_01409 “Process and product innovations aimed at increasing food safety and at diversifying pork-based products” (SAFEMEAT, 2013). It was

funded and run under the call for Research and Competitiveness 2007-2013, decree No. 671, of the Italian Ministry of Education and Research.

The Project leader has been an Italian sausage manufacturing company: Salumificio Dodaro SpA. The Project encompassed Italian partners from industry, University and public research centers, mostly located in the so-called EU “regions of convergence”.

The project proposed and run complex research and industrial activities aimed at the development of new industrial production processes which should be able of guaranteeing food safety and shelf-life improvement of pork-based products. The novel processes were an answer to the emerging sector needs of products diversification and low environmental impacting packaging solutions.

In particular, the research and the industrial development activities were developed along five interconnected pillars:

1) novel analytical methods and technological solutions aimed at evaluating and improving the quality and the safety of meat-based food for the needs of the sector industries such as:

- monitoring and controlling of microbiological and sensorial food quality during the production processes in order to guarantee both high food safety profiles (appropriate for the food export) and effective protection against food-toxins risks;

- limit the development of pathogenic microorganisms thanks to innovative anti-microbic methods both in production/maturation industrial sites as well as in the sausage meat mixtures.

2) new ingredient solutions aimed at:

- reducing the use of chemical additives while guaranteeing the same inhibition action on degenerative processes and on the development of pathogenic microorganisms;

- enriching the finally commercialized products as well as the nutritional and health profiles without causing any sensorial profiles modification

- diversifying the product range in terms of distinction perceivable by the markets taking in account the interactions (microbiological, chemical and sensorial) that occur between meat and the different ingredients

- optimizing the fermentation and maturing processes taking in account the food safety and product characterization and standardization needs.

3) innovative packaging material techniques and solutions (films, trays, etc.) able to:

- increase product shelf-life of fresh products

- reduce environmental impact of packaging material

- allow food product cooking

- improve product packaging presentation

4) development of a new range of ready-to-cook products (RTC-foods) and pork-based sauces thanks to:

- the study and the comparative evaluation of pork/vegetal combinations

- the research and the experimentation on products/ingredients treatments in order to define the appropriate cooking timings and methods
- the research and the experimentation on composition and treatments of sauces in order to guarantee an increased shelf-life and an adequate texture and fluidity

5) development of novel traceability system aimed at introducing automatic data storage of products and raw materials as well as at transferring the data to the retail industry and to the final consumer.

### 1.5 The COMSOL Multiphysics® software

The environment chosen in this work for modeling the ripening of a single sausage was COMSOL Multiphysics®, a software for solving many kinds of scientific and engineering problems.

COMSOL Multiphysics® can be used in many application areas, for example mass transfer or heat transfer.

Using its physics interfaces, various types of studies can be performed (e.g. Stationary and time-dependent (transient) studies or linear and nonlinear studies).

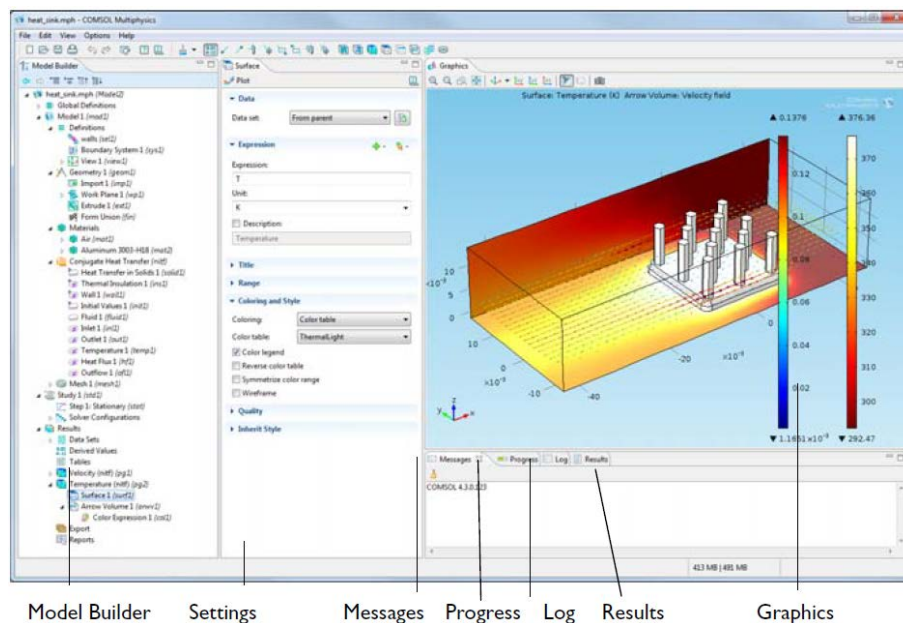


**Figure 3.** The COMSOL Desktop with its major windows in a widescreen layout

When solving the models, COMSOL Multiphysics® uses the proven finite element method (FEM). The software runs the finite element analysis together with adaptive meshing and error control using a variety of numerical solvers.

COMSOL Multiphysics® creates sequences to record all steps that create the geometry, mesh, studies and solver settings, and visualization and results presentation.

Partial differential equations (PDEs) form the basis for the laws of science and provide the foundation for modeling a wide range of scientific and engineering phenomena.

Modeling can be implemented in COMSOL through the integrated Model Builder. It has a tree branch organization and allows to implement a model by selecting the branches in the order suggested by their default positions, from the top down, and defining each branch as needed:

- The Global Definitions branch: for global definitions, for example, defining parameters and functions.
- The Model branches: for defining models. A Model branch includes the associated sub-branches of Definitions, for locally defining parts of the model, Geometry, Materials, Physics, and Meshes. A Model branch includes functionality for local Definitions.
- The Study branch: where the set up study steps and solver configurations are, for solving a model using one or more study types for different analyses.
- The Results branch: for presenting and analyzing results.

# Modeling of salami ripening using a homogeneous approach

## 2.1 Preface

In this thesis chapter, the issue of modeling a single salami ripening in the typical environment of an industrial curing chamber is tackled. For the adoption of a mathematical model and its subsequent implementation in a software code, the approach of considering the sausage as a homogeneous material is followed here. Several different options concerning the description of sausage size, shape and volume variation are taken into considerations, and the corresponding model predictions are discussed and compared.

To this end, the experimental findings provided by various sausage ripening tests carried out at pilot- and industrial scale are employed for discussion and model validation.

## 2.2 Experimental activities

### 2.2.1 Dodaro ripening test

Dodaro SpA conducted a ripening test from 3/3/2015 to 27/3/2015 on a lot of 300 kg of fresh sausage in a curing chamber of industrial scale at Spezzano Albanese, under carefully monitored and controlled conditions for both process and product, as a part of the activities planned in the above mentioned “SafeMeat” project (Various authors, 2013).

The tested product followed the recipe of a typical "non-spicy sausage" (“Salsiccia dolce”) of the Calabria region (Table 2). However, it was added with a functional starter (*Lactobacillus plantarum*, strain 187) developed in the framework of the “SafeMeat” project (Various authors, 2013) and simply manufactured as a straight, near-cylindrical sausage, with a radius  $R_0=20$  mm. Further, the tested product was differentiated in two different experimental “theses”, depending whether the fresh sausages were subjected or not on their outer surface to a fungal inoculum developed within the same “SafeMeat” project (Various authors, 2013).

**Table 2.** *Dodaro recipe of a typical "non-spicy sausage" of the Calabria region*

Ingredients	Quantity (% w/w)
Pork shoulder	80.21
Bacon	16.04
Salt	2.12
Powdered non-spicy pepper	0.96
Fennel	0.19
Starter Hansen	0.01
Dextrose	0.24
E300	0.19
E250	0.01
E252	0.02
Gut	Natural (43/45mm from sow)
Geometry	Cylindrical

An industrial, ascending-flow ripening chamber manufactured by Travaglini SpA was employed for the test.

During the test, the average air conditions in the chamber were temperature = 15 °C, relative humidity = 68 %, air velocity = 0.2 m/s.

Samples were placed at three different elevations (levels) on the racks inside the chamber. For each level, the data referred to product were collected in triplicate. The programming of the curing air conditions throughout the test are reported in Table 3.

**Table 3.** *Ripening program (set points of temperature and relative humidity) of the industrial ripening chamber at the Dodaro SpA factory throughout the test conducted on a lot of 300 kg of a typical "non-spicy sausage"*

Day	Temperature (° C)	Relative Humidity (%)
0	2.5	===
1	21-23	99
2	19-21	65-75
3-5	18-20	66-76
6	14-16	70-80
7	12-14	76-86
8	12-14	70-76
9-24	12-14	70-80

During the test the most important process and product parameters were monitored (Table 4, Table 5, Table 6, Table 7) by the staff at the Dodaro sausage factory, including the features of the products related to drying and maturation as well as growth of mold on their gut. In addition, the sausage shrinkage phenomena were monitored by sequentially measuring the

circumference of the same sample sausage, thus determining the percent reduction in the diameter at each ripening time with respect to the fresh sausage at time 0. For the same purpose, digital photos of samples were taken at various times. The following Figure 4 provides an example of the evolution of the same sample sausage during initial drying and subsequent ripening time.

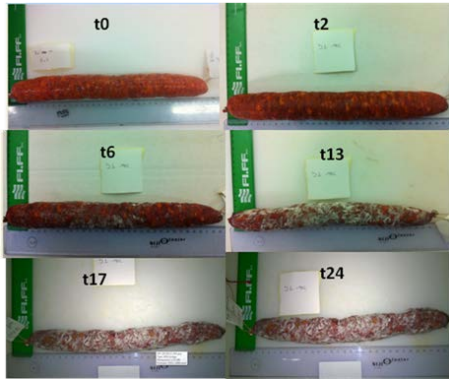


**Figure 4.** Images of the same sausage sampled at ripening days 0, 2, 6, 13, 17, 24 (The radius of the fresh sausage is about  $R_0=20$  mm)

**Table 4.** *Weight (g) of single inoculated and non-inoculated sausage at different levels during the Dodaro ripening test*

Inoculated sausages									
Time (d)	High level			Central level			Low level		
	a1i	a2i	a3i	c1i	c2i	c3i	b1i	b2i	b3i
0	481.2	492.2	488.6	559.8	525.5	504	401	545.9	472
2	457.9	467	464.5	536.7	501.8	481.2	380.3	515.3	446.8
3	420.7	426.9	425.3	499.7	462.5	442.5	349.9	471.2	410.6
6	398.6	350.6	351.9	417.3	382.8	368.9	291.2	388.5	338.4
8	327.6	328.9	329.8	392.8	360	347.2	273.8	365.6	317.8
13	278.1	276.6	276.8	328.4	300.6	291	230	306.8	267.3
15	272.8	272.3	271.2	320.6	294.8	284.7	225.4	301.8	263
17	263	263.5	262.2	309.2	285.1	275.3	218.3	293.3	255.5
20	261.7	262.4	260.9	207.3	283.7	273.9	217.3	292	254.5
24	259.2	260.7	258.8	303.8	281.6	271.2	215.3	289.8	252.8
Non-inoculated sausages									
Time (d)	High level			Central level			Low level		
	a1i	a2i	a3i	c1i	c2i	c3i	b1i	b2i	b3i
0	439.7	508.4	554.8	450.7	569.2	452	488.5	474.1	538.4
2	413.2	479.4	524	429	539.1	428.3	467.1	446.7	503.5
3	379.7	440.8	482.3	396.9	496.8	394.8	431.8	410.1	459.2
6	312.9	364.6	378	333.1	411.1	329.2	362.1	334.7	374
8	293.1	342.2	376.3	313.3	387.2	309.7	340.9	314.1	350.7
13	246.1	289.1	319	264.2	322.9	259.7	287.6	264.7	296.8
15	241.9	284.4	313.6	258.6	317.6	255.4	281.1	261	293.4
17	234.2	275.5	303.9	249.4	307.9	247.3	272	254.1	286.4
20	232.9	274.1	302.3	248.2	306.1	246	270.4	253.1	285.4
24	230.7	272.2	299.9	245.4	303.7	243.9	267.7	251.6	284

**Table 5.** *Circumference (mm) of single inoculated and non-inoculated sausage at different levels during the Dodaro ripening test*

Inoculated sausages									
Time (d)	High level			Central level			Low level		
	a1i	a2i	a3i	c1i	c2i	c3i	b1i	b2i	b3i
0									
2									
3	117	105	113	120	112	115	117	110	105
6	110	98	104	114	102	110	110	103	104
8	107	95	103	112	100	107	108	100	101
13	103	94	100	110	97	105	104	97	98
15	102	94	100	108	96	103	103	97	96
17	102	94	100	106	94	102	102	96	94
20	101	94	100	106	92	101	102	95	92
24	100	95	99	105	92	100	100	95	90
Non-inoculated sausages									
Time (d)	High level			Central level			Low level		
	a1i	a2i	a3i	c1i	c2i	c3i	b1i	b2i	b3i
0									
2									
3	110	110	110	118	118	113	115	110	100
6	101	102	98	113	100	105	112	100	98
8	100	98	97	110	100	105	109	98	98
13	97	95	95	107	97	103	106	95	94
15	96	93	95	107	96	102	105	94	93
17	94	92	94	105	95	100	104	93	92
20	93	91	93	105	94	99	103	92	91
24	92	89	93	104	94	98	102	90	89

From the data in Table 4 and Table 5, the following Table 6 is generated with non-dimensional weight loss and diameter reduction, respectively. Correspondingly, the standard deviations are estimated from the measurements available on all samples at each time.

**Table 6.** %weight loss (WL) and %diameter reduction (DR, from  $D_0=40$  mm) of single inoculated and non-inoculated sausage during the Dodaro ripening test

Inoculated sausages				
Time (d)	Average WL%	Std. dev. WL%	Average DR%	Std. dev. DR%
0				
2	4.9%	0.5%		
3	12.6%	0.9%	10.3%	4.2%
6	26.4%	3.6%	15.6%	4.1%
8	31.9%	1.1%	17.5%	4.2%
13	42.8%	0.8%	19.7%	4.0%
15	43.9%	0.7%	20.5%	3.6%
17	45.7%	0.6%	21.3%	3.6%
20	46.1%	0.4%	21.9%	4.0%
24	46.5%	0.4%	22.5%	3.7%
Non-inoculated sausages				
Time (d)	Average WL%	Std. dev. WL%	Average DR%	Std. dev. DR%
0				
2	5.5%	0.6%		
3	13.0%	0.9%	7.4%	4.2%
6	28.4%	2.0%	8.8%	4.0%
8	32.3%	1.5%	11.4%	3.7%
13	43.0%	1.3%	12.2%	3.8%
15	44.0%	1.1%	13.4%	3.6%
17	45.7%	0.9%	14.2%	3.7%
20	46.0%	0.9%	15.2%	3.5%
24	46.4%	0.8%	7.4%	4.2%

**Table 7.** % moisture content of single inoculated and non-inoculated sausage at different height levels during the Dodaro ripening test

Inoculated sausages					
Time (d)	High level	Central level	Low level	Average	Std. Dev.
0	65.81	68.47	67.41	67.23	1.34
2	66.61	64.9	64.25	65.25	1.22
3	62.66	61.37	63.32	62.45	0.99
6	45.61	49.09	50.23	48.31	2.41
13	34.61	36.53	34.09	35.08	1.29
24	35.88	32.55	35.73	34.72	1.88
Non-inoculated sausages					
Time (d)	High level	Central level	Low level	Average	Std. Dev.
0	65.99	68.05	66.15	66.73	1.15
2	66.48	65.56	65.47	65.84	0.56
3	63.55	64.97	65.59	64.70	1.05
6	50.02	51.85	51.48	51.12	0.97
13	35.04	36.64	37.3	36.33	1.16
24	28.5	30.66	31.18	30.11	1.42

### 2.2.2 SSICA ripening test

Other experimental data were obtained from ripening of innovative salami with a modified recipe to achieve a lower content of animal fat.

Within the same project "Safemeat", the University of Foggia developed a sausage recipe with reduced content in animal fat and functional starter (Table 8), starting from the original Dodaro sausage recipe. In the EVO sausages the 60% of animal fat was replaced with extra virgin olive oil (EVO) trapped in a protein foam (protein whey and potato starch).

The Dodaro S.p.A. carried out the production of the EVO sausage paste using the recipe and the equipment for the normal production (Figure 5).

The *Stazione Sperimentale per l'Industria delle Conserve Alimentari* (SSICA), as a consultant for the Safemeat project, conducted N.4 tests of ripening of the "innovative" meat products of interest to the project in the instrumented pilot-scale chamber in Parma (Various Authors, 2013).

In this thesis, the experimental results and data to be used for the simulations come from the SSICA test No. 3 and 4.

Each lot consisted of 110 kg of fresh product (50% of standard + 50% of EVO sausage) sent from Dodaro to SSICA (Parma) where it was cured in the pilot cell based on the "air flow from bottom upward" forced air circulation. The ripening conditions were based on the experience of the operator who set up and regulated the necessary parameters of curing air.

During the test No. 3, carried out from 17/3/2015 to 8/5/2015, the average air conditions in the chamber were temperature = 12°C, relative humidity =

57%, air velocity = 0.2 m/s. The experimental data of this test useful for the simulation work are shown in the Table 9 and Table 10.

During the test No. 4, carried out from 24/6/2015 to 31/8/2015, the average air conditions in the chamber were temperature = 7°C, relative humidity = 54%, air velocity = 0.2 m/s. The experimental data of this test useful for the simulation work are shown in the Table 10 and Table 12.

**Table 8.** *Recipe of "EVO sausage"*

Ingredients	Quantity (% w/w)
Pork shoulder	78.05
Bacon	6.24
Extra virgin olive oil	9.37
Protein foams	2.41
Enzyme	0.28
Salt	2.06
Powdered non-spicy pepper	0.94
Fennel	0.19
Starter Hansen	0.01
Dextrose	0.23
E300	0.19
E250	0.01
E252	0.02
Gut	Natural (43/45mm from sow)
Geometry	Cylindrical



**Figure 5.** *Images of EVO sausages at the startup of the ripening test*

**Table 9.** *Weight (g) of rack sticks at different levels for the SSICA test No. 3 (each stick carries 10 sausages of either EVO or traditional type)*

Time (d)	EVO sausages			Traditional sausages		
	High l.	Central l.	Low l.	High l.	Central l.	Low l.
0	5337	5153	5207	5035	5438	5208
1	5136	4953	4963	4696	4989	4751
2	5036	4869	4860	4492	4748	4510
3	4972	4811	4793	4371	4602	4363
6	4820	4677	4652	4116	4370	4137
7	4782	4640	4617	4055	4310	4082
8	4724	4595	4566	3956	4217	3992
9	4681	4558	4523	3877	4142	3919
10	4629	4513	4474	3785	4043	3826
14	4465	4366	4310	3480	3731	3535
17	4348	4261	4198	3277	3522	3340
21	4205	4130	4053	3069	3305	3141
28	3965	3906	3813	2861	3046	2885
31	3876	3821	3723	2771	2964	2800
37	3716	3666	3564	2701	2881	2702
42	3599	3547	3446			
49	3452	3411	3313			
52	3410	3357	3267			

From the data in Table 9, the following Table 10 is generated with non-dimensional weight loss.

**Table 10.** % weight loss for an average single sausage in the SSICA test No. 3 on EVO (initial mass 523.2 g) and traditional (initial mass 522.7 g) sausages

Time (d)	EVO sausages	Traditional sausages
0	0.0	0.0
1	4.1	7.9
2	5.9	12.3
3	7.1	15.0
6	9.9	19.5
7	10.6	20.6
8	11.5	22.4
9	12.3	23.9
10	13.3	25.7
14	16.3	31.5
17	18.4	35.3
21	21.1	39.3
28	25.6	43.9
31	27.2	45.6
37	30.3	47.2
42	32.5	
49	35.2	
52	36.1	

**Table 11.** Weight (g) of rack sticks at different levels for the SSICA test No. 4 (each stick carries 10 sausages of either EVO or traditional type)

Time (d)	EVO sausages		Traditional sausages	
	High l.	Central l.	High l.	Central l.
0	4830	4846	5052	5028
1	4675	4710	4853	4813
2	4564	4619	4674	4586
5	4369	4438	4244	4142
6	4323	4393	4141	4050
7	4270	4348	4061	3970
8	4220	4305	3975	3888
9	4184	4271	3890	3810
14	3990	4106	3575	3469
21	3777	3896	3217	3155
36	3400	3514	2820	2787
40	3326	3433	2716	2709
49	3204	3304		
68	3060	3115		

From the data in Table 11, the following Table 12 is generated with non-dimensional weight loss.

**Table 12.** % weight loss for an average single sausage in the SSICA test No. 4 on EVO (initial mass 483.8 g) and traditional (initial mass 504.0 g) sausages

Time (d)	EVO sausages	Traditional sausages
0	0.0	0.0
1	3.0	4.1
2	5.1	8.1
5	9.0	16.8
6	9.9	18.7
7	10.9	20.3
8	11.9	22.0
9	12.6	23.6
14	16.3	30.1
21	20.7	36.8
36	28.5	44.4
40	30.1	46.2
49	32.7	
68	36.2	

### 2.3 Mathematical modeling

The mathematical model first adopted and then modified here is that previously published by Diaferia et al. (2011).

They considered 1D, axis-symmetric, infinitely long and time-fixed cylindrical geometry; homogeneous and isotropic material; no distinction between the inner part (core) and the casing; water concentration as a distributed parameter; the internal water transfer rate as a concentration-dependent Fickian diffusion with the assumption of an effective diffusion coefficient  $D_e$  depending on the local water content (Imre and Kornyei, 1990).

Diaferia et al. (2011) developed and validated their mathematical model able of predicting drying features and temperature history of a single sausage, under both natural and forced air circulation.

Figure 6 shows the infinitesimal control volume the model uses for the mass and energy balance equations.

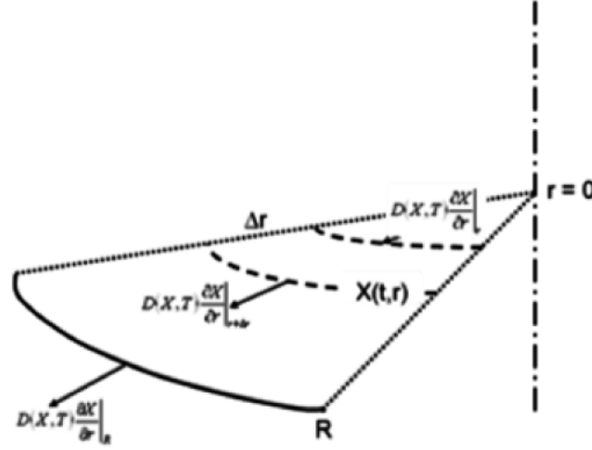


**Figure 6.** Geometry of the mathematical model for mass balance and energy balance

The mass balance and its initial and boundary conditions are:

$$\frac{\partial X}{\partial t} = \frac{D(X,T)}{r} \frac{\partial X}{\partial r} + \frac{\partial}{\partial r} \left( D(X,T) \frac{\partial X}{\partial r} \right) \quad (1)$$

$$I. C. : X(0, r) = X_0$$

$$B. C. : \begin{cases} \left( \frac{\partial X}{\partial r} \right)_{r=0} = 0 \\ -\rho_{ds} D(X,T) \left( \frac{\partial X}{\partial r} \right)_{r=R} = N_R M_w \end{cases}$$

where:

X= moisture content on dry basis;

t= time;

D(X,T)= diffusivity of water in solid;

T= temperature;

r= radius;

$\rho_{ds}$ = dry solid density;

$M_w$ = water molar weight;

$$N_R = k_c \left[ \frac{a_{we}(X(R, t)) \cdot p^*(T(t))}{\mathfrak{R}T(t)} - \frac{RH \cdot p^*(T_a)}{\mathfrak{R}T_a} \right];$$

$N_R$ = mass flux;

$k_c$ = mass transfer coefficient (m/s) according to Diaferia et al. (2011);

$a_{we}$ = equilibrium water activity on the surface;

$p^*$ = water vapor pressure;

$\mathfrak{R}$ = gas constant;

RH= air relative humidity;

$T_a$ = air temperature.

The effective diffusion coefficient  $D_e$  is that adopted by Imre and Kornyei (1990) and shows a strong dependence from the local water content ( $X$ ), apart from temperature ( $T$ ).

$$D = [1.75 + 8.4 \cdot 10^{-5} \cdot (T - 273)^{3.4}] \cdot \exp[(X - 0.2) \cdot 0.69] \cdot 10^{-11} \cdot \max \left[ 1; \frac{(T - 273)}{17} \right] \cdot \{1 + \max[0; 0.06 \cdot (X - 0.6) \cdot (T - 273)]\}$$

The Oswin law, widely used in the food sector as moisture desorption curve, is the adopted correlation between  $X$  and  $a_{we}$ :

$$X(R, t) = K \left( \frac{a_{we}}{1 - a_{we}} \right)^n \quad (2)$$

where  $K$  and  $n$  are tabulated parameters for different types of salami (Diaferia et al., 2011).

The energy balance and its initial and boundary conditions are:

$$\rho c_p \frac{\partial T}{\partial t} + \rho c_p u \cdot \nabla T + \nabla(-k \nabla T) = 0 \quad (3)$$

$$I. C.: T(0, r) = T_0$$

$$B. C.: \begin{cases} \left( \frac{\partial T}{\partial r} \right)_{r=0} = 0 \\ -k \left( \frac{\partial T}{\partial r} \right)_{r=R} = q_R \end{cases}$$

where:

$\rho$ = sausage density;

$c_p$ = heat capacity;

$u$ = average velocity of air stream “bathing” the products;

$k$ = thermal conductivity;

$$q_R = h(T_a - T) + \varepsilon \sigma (T_\infty^4 - T^4) - N_R M_w \Delta H(T);$$

$q_R$ = thermal flux;

$h$ = energy transfer coefficient according to Diaferia et al. (2011);

$\varepsilon=0.76$  sausage emissivity for a grey body;

$\sigma$ = Stefan-Boltzmann constant;

$T_\infty$ = chamber wall  $T$ , assumed equal to  $T_a$ ;

$\Delta H(T)$ = enthalpy of vaporization.

The thermal-physical parameters are those presented and discussed in Diaferia et al. (2011).

Actually, sausages do not have a time-invariant volume, but exhibit a shrinking size mostly due to drying.

Further, salami may have a quite irregular shape or originally be a geometric solid other than the cylinder.

Therefore, a reliable mathematical model has to take into account the above-mentioned issues and provide reasonable predictions for them.

## 2.4 Comsol Multiphysics® code implementation

COMSOL Multiphysics® can be used in many application areas, for example fluid dynamics and heat transfer.

Both the “mass transfer in diluted systems” and “heat transfer in solids” physics were adopted to develop a code in COMSOL Multiphysics®.

The governing equations, i.e., the water mass (1) balance and the energy balance (2), both expressed in terms of Partial Differential Equations (PDEs) with their boundary and initial condition, were solved by COMSOL by means of the Finite Element Methods (FEM).

The initial and boundary conditions described in mathematical model were applied to the adopted physics.

The implementation of a calculation code started from the development of a perfect cylindrical 2D axi-symmetric geometry to have a low computational weight (see Figure 7A).

The used mesh for the simulation is of the Mapped type with calibrated dimension for General physics Extremely fine (see Figure 7B).

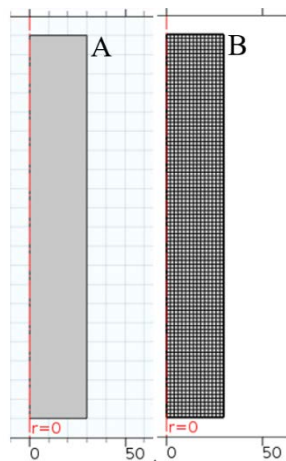


**Figure 7.** *Cylindrical 2D axi-symmetric geometry (A) and mesh (B)*

Properties of the software built-in materials were not used, but all the characteristics of the salami were implemented in Parameters in Global definitions (if parameters) or in Variables as Definitions (if variables depending on the moisture content or temperature).

The implementation was finalized in two different code versions in order to separately account either forced or natural convection for mass and heat transfer. In particular, this was required because, depending on the type of convection, some parameters (e.g., the dimensionless numbers in transfer coefficients) must be calculated with different formulas.

However, weight loss is essentially due to the contribution of forced convection and natural convection has the only purpose of allow a

redistribution of the water content inside the salami. The two phases, i.e., forced and natural air circulation, alternate in an unscheduled manner, closely related to the experience and sensitivity of the operator, who can also change the temperature, velocity and relative humidity of the air in the ripening chamber. For this reason, it was decided to develop a predictive model that has ripening conditions in input with the only forced convection as averaged throughout the whole ripening time.

The COMSOL code needs specific input data for the ripening of a particular kind of salami.

This code has been validated against previous literature data concerning the “Turista Buonpiemonte” sausage, which was manufactured by the Raspini company as a typical small-size sausage of the Piedmont region and was ripened during an experimental program in the pilot-scale, ascending-flow chamber located in Parma (DRIP, 2000). The Figure 8A shows a commercial view of the product that is representative of the Turista dry sausage.

In particular, thanks to its typical shape, a specific study was carried out on the Turista Buonpiemonte (Figure 8A) to evaluate the effect of the shape on the weight loss prediction.

Running the code requires as input data the initial properties of the fresh sausage and the curing air conditions, i.e., temperature, relative humidity and velocity. So, as an input to the model, the data related to the ripening of the Turista type salami were used, i.e., the values reported in DRIP (2000). They were obtained by properly averaging the data acquired by the chamber supervision system throughout the test duration.

**Table 13.** Code data input for Turista salami ripening

Name	Value	Description
$T_{\text{air}}$	289.03 K	Air temperature
$T_0$	278.15 K	Initial salami temperature
$X_{r0}$	0.5371	Initial salami moisture fraction
$m_t$	600 g	Initial salami weight
$L$	200 mm	Salami length
$D$	60 mm	Salami diameter
RH	0.7847	Air relative humidity
$k_{\text{oswin}}$	0.074638	K Oswin constant
$n_{\text{oswin}}$	0.939	n Oswin constant
$u$	0.6 m/s	Average velocity of air stream “bathing” the products
Duration	14 d	Overall length of the ripening test
Step	1 d	Calculation step

The other parameters with dependencies from temperature and water concentration are literature correlations (Perry et al., 1998).

An improvement of the cylindrical geometry is provided by the adoption of an irregular domain with two approaches. The first one is still axi-

symmetric and generates a solid domain by overlapping three ellipsoids. In practice, this corresponds to the actual shape of a typical Italian “soppressata”. Boolean operations of union and subtraction of sets (ellipsis) are needed for the realization of the domain. A further adjustment is the use of a “non-mapped mesh” in COMSOL due to the irregularity of the domain.

Figure 8B shows the used 2D axi-symmetric geometry with the respective mesh (Figure 8C) of the type Free triangular with calibrated dimension for General physics Extremely fine of Figure 7B.

A second approach is that of developing an irregular domain without the symmetry axis and with a non-symmetric solid shape. In practice, this corresponds to the actual shape of a curved sausage. In this case, modeling in 2D is no more possible, and a 3D domain is required. The 3D formulation has hampered the model by increasing the degrees of freedom and imposing constraints on the mesh. In particular, a mesh of unstructured tetrahedral and a characteristic mesh size larger than that used in the previous cases were required to reduce the calculation load and to achieve convergence in a reasonable time.

Figure 8D shows the built irregular 3D geometry with the respective mesh (Figure 8E) for the simulation of the type “Free tetrahedral” with calibrated dimension for General physics Extra fine.

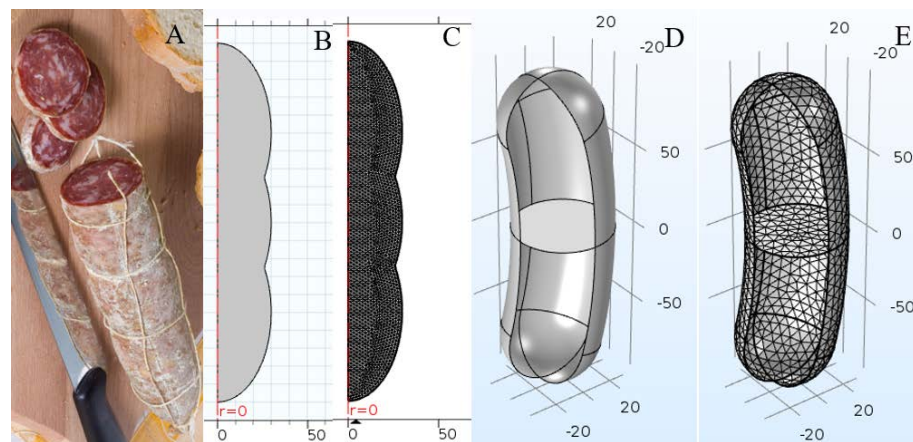


**Figure 8.** Image of a ready-to-eat Turista dry sausage (A) compared to various geometric representations: irregular 2D axi-symmetric (B) and its mesh (C), irregular 3D geometry (D) and its mesh (E)

In order to account for the effects of sausage shrinkage (due to water removal) during ripening, a further physics has been invoked in COMSOL i.e., the “moving mesh” on a Free deformation domain. For the sake of simplicity, the cylindrical domain was assumed to undergo radial deformation only, i.e., the edge could move backward in the radial direction only (a “moving boundary” approach). The two-dimensional and axi-symmetric

model in cylindrical geometry was chosen as the domain for implementation of the “moving mesh” physics. This choice partly compensates the increased load in calculation resources and time needed to approach convergence.

The “moving mesh” physics requires a constitutive equation describing the rate of edge receding as a function of the residual water content. No quantitative relationship concerning salami was found in literature. Therefore, the following correlation proposed by Feyissa et al. (2009) in the case of meat roasting has been adopted.

$$R(t) = R_0 \left( 1 - \frac{\beta \cdot V_{w,l}(t)}{V_0} \right)^{\frac{1}{3}} \quad (4)$$

where:

R= external radius;

$\beta$ = shrinkage coefficient;

$V_{w,l}$ = volume of lost water;

$V_0$ = initial sausage volume.

$\beta=1$  was taken implying that no porosity in the sausage was generated at all in place of the removed water. The time derivative of the Eq. (4) provides the surface receding rate.

The model with volume shrinkage was validated on the sausage coming from the Dodaro test because the Dodaro investigators sampled the circumference of the sausage, a datum that is not monitored usually.

Running the code requires as input data the initial properties of the fresh sausage and the curing air conditions. So, as input to the model, the data related to the ripening of the non-spicy Sausage in Dodaro factory were used:

**Table 14.** Code data input for the Dodaro sausage ripening

Name	Value	Description
$T_{air}$	288.05 K	Air temperature
$T_0$	278.15 K	Initial salami temperature
$X_{r0}$	0.67	Initial salami moisture fraction
$m_t$	497 g	Initial salami weight
L	430 mm	Salami length
D	40 mm	Salami diameter
RH	0.68	Air relative humidity
$k_{oswin}$	10.8e-2	K Oswin constant
$n_{oswin}$	0.43	n Oswin constant
U	0.2 m/s	Average velocity of air stream “bathing” the products
Duration	24 d	Overall length of the ripening test
Step	1 d	Calculation step

A further simulation was set up with data from the tests No. 3 and 4 carried out in Parma by SSICA on two EVO sausage ripening tests and their

respective traditional control samples. The inputs for the simulations are shown in Table 15.

**Table 15.** Code data input for EVO and traditional sausage ripening (SSICA tests No. 3 and 4)

Name	Test NO. 3		Test NO. 4		Description
	EVO	Trad.	EVO	Trad.	
T <sub>air</sub>	285.15 K	285.15 K	280.15 K	280.15 K	Air temperature
T <sub>0</sub>	278.15 K	278.15 K	278.15 K	278.15 K	Initial salami temperature
X <sub>r0</sub>	0.67	0.67	0.67	0.67	Initial salami moisture fraction
m <sub>t</sub>	523.2 g	522.7 g	483.8 g	504.0 g	Initial sausage weight
L	430 mm	430 mm	430 mm	430 mm	Sausage length
D	40 mm	40 mm	40 mm	40 mm	Sausage diameter
RH	0.57	0.57	0.54	0.54	Air relative humidity
k <sub>oswin</sub>	10.8e-2	10.8e-2	10.8e-2	10.8e-2	K Oswin constant
n <sub>oswin</sub>	0.43	0.43	0.43	0.43	n Oswin constant
u	0.2 m/s	0.2 m/s	0.2 m/s	0.2 m/s	Average velocity of air stream “bathing” the products
Duration	52 d	36 d	68 d	40 d	Overall length of the ripening test
Step	1 d	1 d	1 d	1 d	Calculation step

The development of the codes and the simulation runs have been carried out with a MS Windows workstation based on the Intel® Core™ i7-6700HQ processor with 2.60 GHz clock rate and 32 GB RAM.

## 2.5 Simulation results

Drying in a unique phase was considered under forced air circulation, that is a condition corresponding to values of air temperature, relative humidity and velocity as averaged over the whole duration of the ripening test. Based on measurements, the value required for air velocity is just the average velocity of the uprising air stream “bathing” the hung products.

With the simulation of the Dodaro salami (Figure 10), evaluating the effect of volume contraction on the prediction was possible. On the other side, with the simulation of the drying of the Turista salami (Figure 14), evaluating the effect of the variation of shape on the predictive prowess of the calculation code was possible.

The developed COMSOL code allows obtaining time and space profiles of the dependent variables in an easy and fast way, with a clear and meaningful graphical representation.

The considerations on the graphs produced by the calculation code can be extended to all the simulations; for this reason, in this part of the work, the most significant graphs concerning the simulation of the Dodaro salami ripening are commented.

The following Figure 9 is an example of the way the profile of water concentration can be graphically reported as a function of time from the center to the surface of the sausage. In particular, it was preferred to represent time on a day-by-day scale, although this is not mandatory in the COMSOL code implementation.

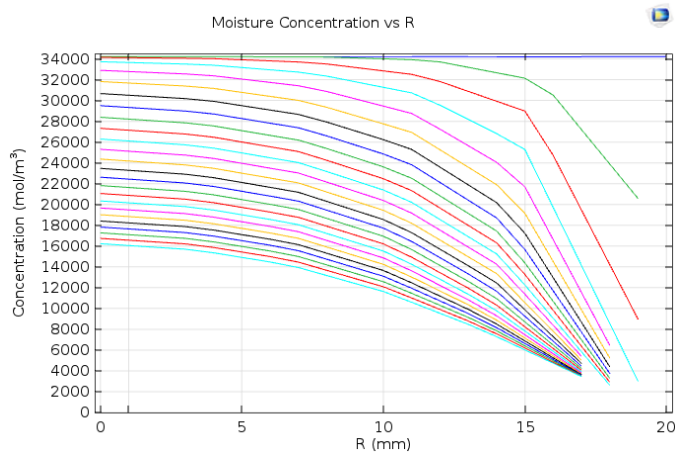


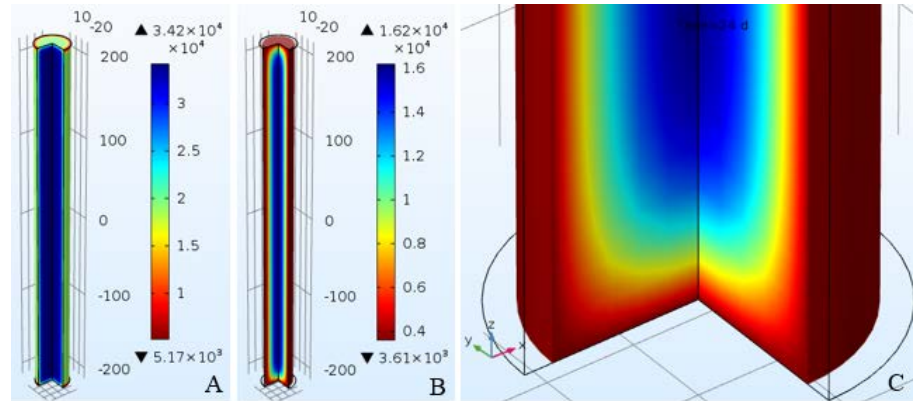
**Figure 9.** Water concentration ( $\text{mol/m}^3$ ) profile as a function of the radial position ( $R$ ) parametrically in the ripening day. (Dodaro test 2015: Simulation in axis-cylindrical geometry with moving mesh)

First of all, Figure 9 undoubtedly confirms that the water concentration has to be intended as a “distributed parameter” variable in the investigated mechanism. In particular, Figure 9 clearly shows how the water concentration profile is gradually lowered day by day and how the outer radial position is receding back due to the shrinking phenomenon.

Figure 10 show the 3D color plot of the water concentration ( $\text{mol/m}^3$ ) in the Dodaro sausage in a given ripening day, precisely at both extremes of the ripening test, that is the end of day 1 (Figure 10A) and that of day 24 (Figure 10B).

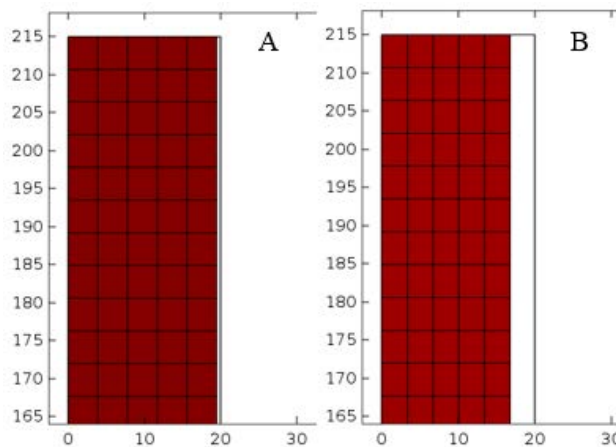
The change in the color scale, which was determined by the software to distinguish small variations, apparently makes the change in the water concentration profile sharper at the day 24 than at the day 1: it is not so, as better demonstrated by the corresponding profiles in Figure 9. Further, the 3D

color plots do report the outer radial position recession, which is more evident in the zoom of Figure 10C, of course.



**Figure 10.** 3D plot of the water concentration ( $\text{mol}/\text{m}^3$ ) in the sausage at day 1 (A), at day 24 (B) and at day 24 with zoom on the edge (C) (Dodaro test 2015: Simulation in 2D axi-cylindrical geometry with moving mesh)

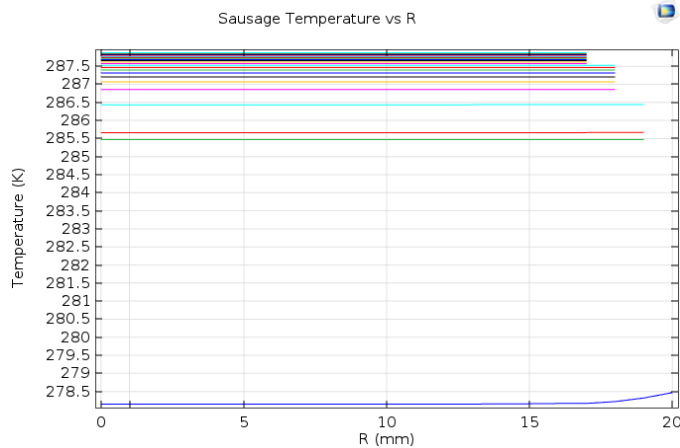
Figure 11 clearly shows how the moving mesh physics involves a contraction of the domain (2D axi-symmetric cylinder) between day 1 and day 24 of the ripening simulation with, in this case, a boundary speed dependent by the correlation of Feyissa.



**Figure 11.** Zoom of mesh decrease in 2D domain from day 1 (A) to day 24 (B) during simulation of sausage ripening (Dodaro test 2015)

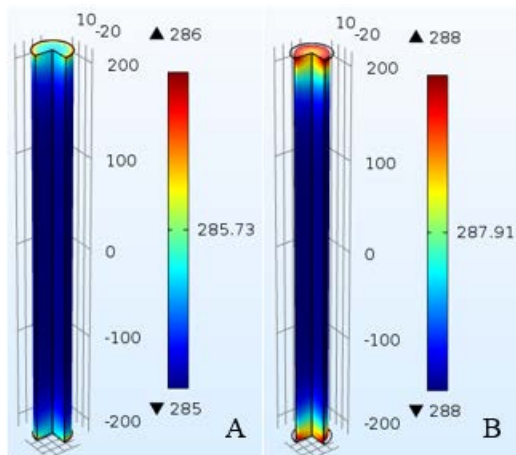
Similarly to the previous ones, the next Figure 12 and Figure 13 graphically report the temperature profile as a function of time from the center to the surface of its outer surface.

Figure 12 seems to demonstrate that, although sausage temperature has been modeled as a “distributed parameter” variable, its actual variation with the radius is negligible.



**Figure 12.** Temperature (K) profile as a function of the radial position (R) parametrically in the ripening day. (Dodaro test 2015: Simulation in 2D axi-cylindrical geometry with moving mesh)

This is further made evident by the 3D color plots in Figure 13, where the apparent change in the color scale, which was determined by the software, is instead within an order of magnitude of 0.1 K at both extremes of the ripening test, that is the end of day 1 (Figure 13A) and that of day 24 (Figure 13B). Only the initial temperature profile (see the blue line at the bottom of Figure 12) departs from a flat pattern.



**Figure 13.** 3D plot of the temperature (K) in the sausage at day 1(A) and at day 24 (B) (Dodaro test 2015: Simulation in 2D axi-cylindrical geometry with moving mesh)

Therefore, it can be stated that sausage temperature can be considered as a “lumped parameter” variable in the investigated mechanism, at least under the conditions of the experimental test to which the present simulation refers.

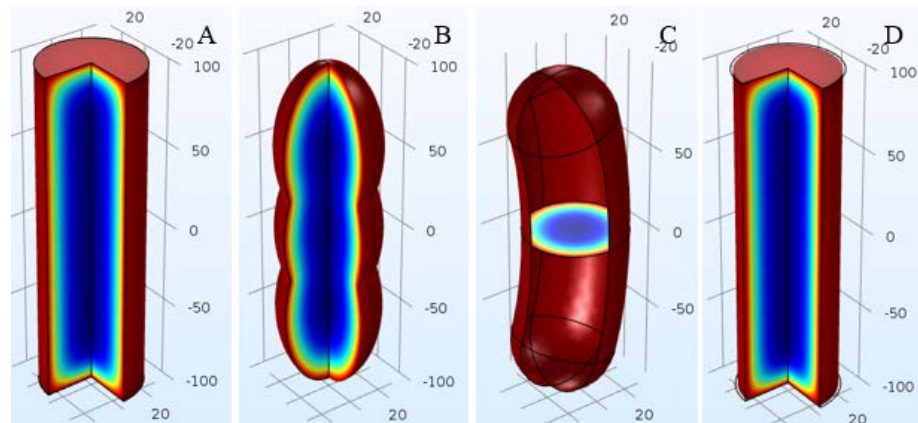
In addition, Figure 12 shows how the temperature profile is gradually raised day by day, although in a quite narrow range (from about 286 to 288 K) and how evident the outer radial recession is.

Figure 13 seem to show a vertical “edge effect”, i.e., a temperature gradient at the lower and upper base of the cylindrical sausage; however, this latter is visible on the basis of the software-determined color scale, but negligible as far as its actually calculated order of magnitude.

With regard to the graphs of the simulation results, the above considerations are valid also for the simulation of the curing of the Turista salami with irregular shape (Figure 14).

## 2.6 Comparison between predicted and experimental results

The validation of the irregular shape model code has been pursued thanks to literature data, i.e., by taking the Turista Buonpiemonte as a reference sausage from the previously mentioned DRIP project (2000).



**Figure 14.** 3D color maps representing the predicted water concentration at the very end of Turista salami ripening in A) cylindrical 2D axis-symmetric geometry, B) irregular 2D axis-symmetric geometry, C) irregular 3D geometry, D) cylindrical 2D axis-symmetric geometry with shrinking

Just as a first impact of the simulation work, the Figure 14 reports 3D color maps of the predicted water concentration at the very end of Turista salami ripening for the various options considered for salami shape, i.e., A) cylindrical 2D axis-symmetric geometry, B) irregular 2D axis-symmetric geometry and C) irregular 3D geometry. In addition, the Figure 14D graphically shows the effect of salami shrinking in the cylindrical 2D axis-symmetric geometry. It shows how the radial moisture concentration profiles,

evaluated according to the color gradation, do not change with the variation of the shape.

To provide a quantitative assessment of the model predicting capability, attention has been focused on the sausage weight loss, which is the easier to check product variable and the most well-known performance index in industrial salami production. The code predictions of the Turista weight loss under forced air circulation are reported as a function of the ripening time, together with the experimental data, in the following figures.

For the cylindrical 2D axi-symmetric geometry (Figure 15) there is a very good prediction of the final weight loss, i.e., at the end of the maturation, whereas a larger discrepancy in comparison to the experimental data appears in the initial part of the simulation. The value of the Root Mean Square Error calculated from the experimental and predicted sausage weight losses is  $RMSE=1.81$ .

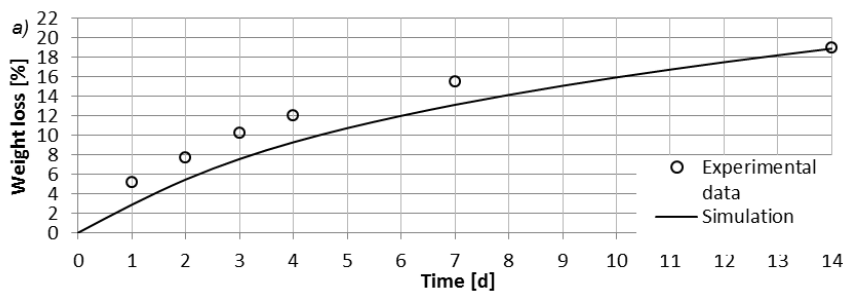


**Figure 15.** *Experimental and simulated weight loss for cylindrical 2D axi-symmetric geometry (Turista Buonpiemonte reference sausage)*

For the irregular 2D axi-symmetric geometry (Figure 16) there is a slight increase in the prediction of the final weight loss, whereas the deviation between predicted and experimental values remains in the initial part of the simulation. In this case it is  $RMSE=2.40$ .

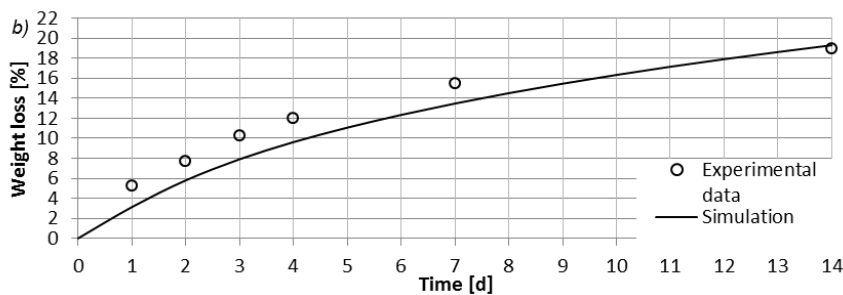


**Figure 16.** *Experimental and simulated weight loss for irregular 2D axi-symmetric geometry (Turista Buonpiemonte reference sausage)*

Predictions based on the irregular 3D geometry (Figure 17) show negligible difference and just the same trend of the previous case. In this case it is  $RMSE=2.08$ .

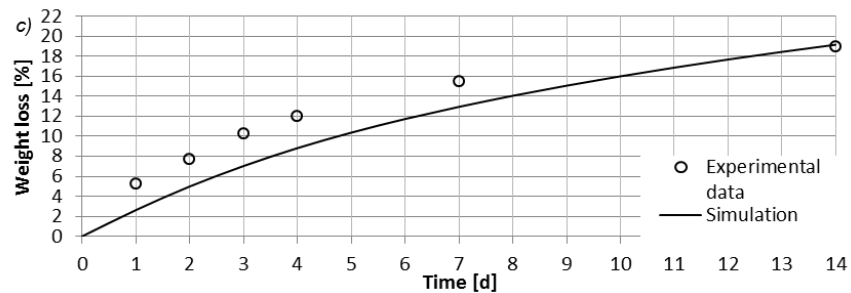


**Figure 17.** Experimental and simulated weight loss for irregular 3D geometry (Turista Buonpiemonte reference sausage)

For the cylindrical 2D axi-symmetric geometry with volume shrinking (Figure 18) there is a better overall performance in the prediction of weight loss throughout the ripening time.

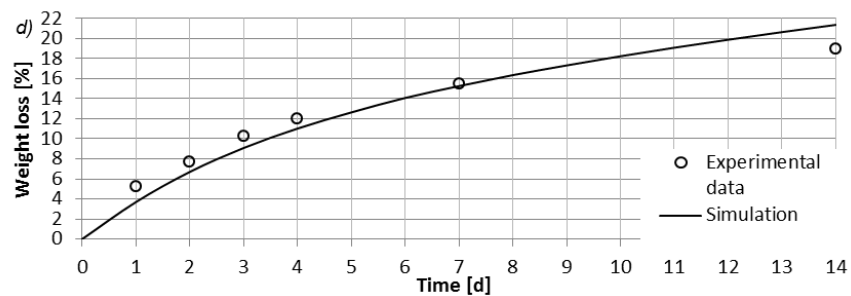


**Figure 18.** Experimental and simulated weight loss for cylindrical 2D axi-symmetric geometry with shrinking (Turista Buonpiemonte reference sausage)

In particular, the agreement of the experimental data and the simulation is better in the first week, but the final predicted weight loss is higher than both the experimental datum and the values calculated with the previous model geometries. A value  $RMSE=1.28$  confirms that accounting for shrinking in a simple cylindrical 2D axi-symmetric geometry gives the best prediction performance over the whole ripening time for the Turista Buonpiemonte reference sausage.

A further code validation was made with the results of the previously mentioned ripening test carried out at Dodaro SpA.

Figure 19 reports the comparison between experimental and predicted single sausage weight loss in cylindrical 2D axi-symmetric geometry obtained according to the moving mesh (with shrinking) as opposed to the time-invariant case (without shrinking). The experimental data are provided in 2 different sets for Inoculated (I) and Not-Inoculated sausages (NI), each averaged over several samples. It is worth noting that inoculation caused no actual difference on the weight loss of the sausage samples. Actually, the measurements are very close to each other at each ripening day for both Inoculated (I) and Non-Inoculated sausages (NI) that all underwent a relevant surface covering by molds (Figure 4), a well-known phenomenon that is not expected to appreciably affect the weight loss. All in all, the prediction of the sausage weight loss turns out satisfactory. The simulated curves appear close enough to the experimental data in both instances A) and B) of Figure 19 in spite of the underlying assumption of a unique value (averaged conditions) of air temperature, relative humidity and velocity throughout the whole duration of the test.

The prediction based on the 2D time-invariant geometry with no shrinking slightly overestimates the experimental data at the last ripening day (i.e., 24th). In this case it is  $RMSE=2.30$ . The prediction based on the 2D moving-mesh geometry with shrinking appears slightly worse ( $RMSE=4.61$ ) and with a trend to overestimate the experimental data at the day 24. This does not mean that taking shrinking into consideration makes the model less reliable in predicting phenomena related to drying; likely, shrinking is correctly taken into account, but the correlation by Imre and Kornyey (1990) for the effective diffusion coefficient  $D_e$  is not fully adequate in predicting the internal water transfer rate for the Dodaro “non-spicy sausage”.

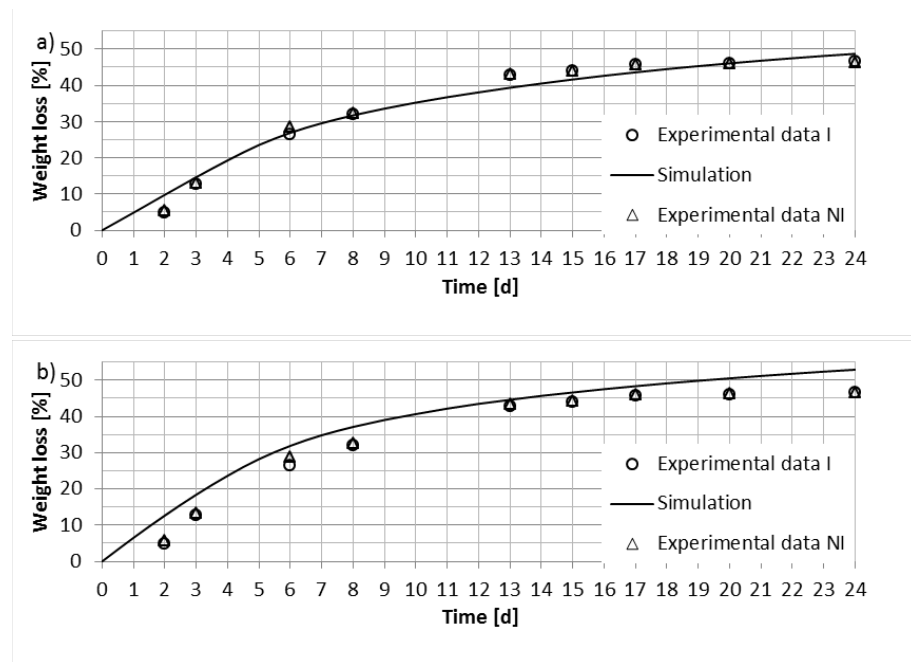


**Figure 19.** Comparison between experimental and predicted sausage weight loss in cylindrical 2D axis-symmetric geometry. Dodaro test 2015: model predictions a) without shrinking; b) with shrinking (I: set of experimental data for mold Inoculated sausages; NI: set of experimental data for Non-Inoculated sausages)

Similar to the previous one, Figure 20 reports the comparison between the experimental water mass fraction (%) and the volume-averaged water content (%) as predicted in the cylindrical 2D axis-symmetric geometry either with the moving mesh or without consideration of shrinking. Again, the experimental data are provided in 2 different sets for Inoculated (I) and Non-inoculated sausages (NI), each averaged over several samples.

The prediction of the water mass fraction in the sausage turns out encouraging. All in all, the simulated curves appear a bit distant from the experimental data in both instances a) and b) of Figure 20. This outcome can be attributed to the assumption of a unique ripening phase in the simulations, i.e., with constant air conditions.

Differently from the previous discussion on weight loss, the simulation curve provided by the 2D moving-mesh geometry with shrinking (RMSE=3.14) appears to better reproduce the experimental trend than the prediction with no shrinking (RMSE=4.90).

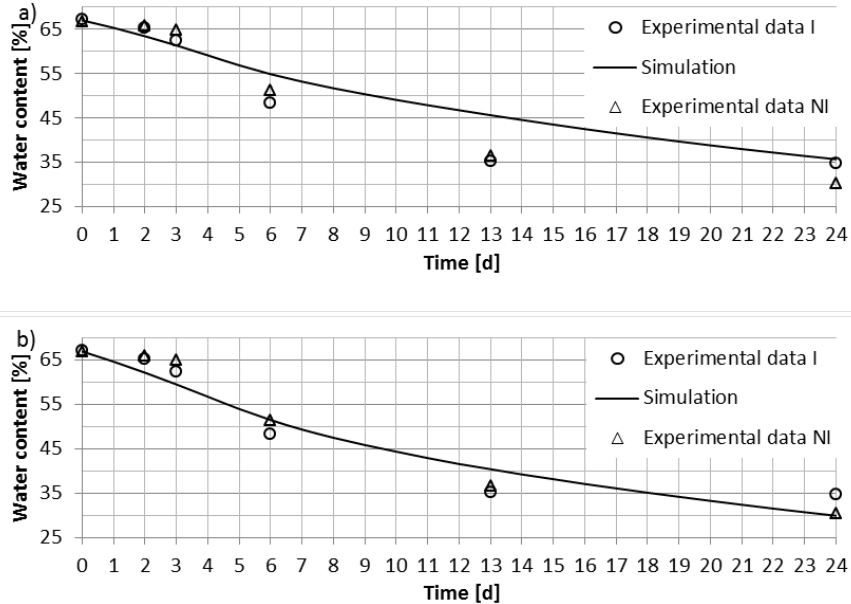


**Figure 20.** Comparison between experimental and predicted sausage water content in cylindrical 2D axi-symmetric geometry. Dodaro test 2015: model predictions a) without shrinking; b) with shrinking (I: set of experimental data for mold Inoculated sausages; NI: set of experimental data for Non-Inoculated sausages)

The simulation with moving mesh provides a further opportunity of model validation with respect to the reference case with no shrinking. Figure 21 shows the comparison between experimental and predicted single sausage shrinkage curves by reporting the % reduction in the diameter at each ripening time with respect to the fresh sausage at time 0. Again, the experimental data are provided in 2 different sets for Inoculated (I) and Non-inoculated sausages (NI), each averaged over several samples.

Obviously, the simulation carried out according to the approach without a moving mesh yields a null shrinkage (see the horizontal dashed line in Figure 21). The shrinkage curve calculated by the 2D axi-symmetric cylindrical geometry with the moving mesh has a reasonable growing trend, but it tends to underestimate the actual experimental data. The Root Mean Square Error calculated from the experimental and predicted diameter shrinkage data turns out RMSE=4.13%.

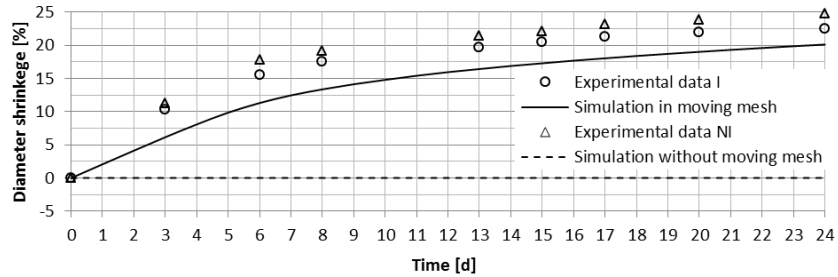


**Figure 21.** Comparison between experimental and predicted diameter shrinkage curves in cylindrical 2D axis-symmetric geometry. Dodaro test 2015: model predictions without shrinking (dashed line) and with shrinking (solid line) (I: set of experimental data for mold Inoculated sausages; NI: set of experimental data for Non-Inoculated sausages)

A further code validation was made with the results of the previously mentioned ripening test No. 3 and 4 carried out at SSICA with EVO and traditional sausages (used as control samples in the tests). In all simulations, calculations were carried out by keeping the 2D axi-symmetric cylindrical geometry and considering volume shrinking.

The prediction of the weight loss for traditional sausages is satisfactory test for SSICA test No. 3 (RMSE=3.35 in Figure 22A), whereas exhibits a more pronounced underestimation for SSICA test No. 4 (RMSE=5.42 in Figure 23A).

In the case of EVO sausages (Figure 22B, Figure 23B), in order to have a more reasonable prediction (RMSE=4.30 and RMSE=2.02, respectively), it was necessary to introduce a corrective factor (equal to 0.45) in the diffusivity expression by Imre and Kornyey (1990), which takes into account the decrease in moisture diffusion due to the presence of olive oil in the product.

The reduction of the operating temperature down to 7 °C in the SSICA No. 4 test determined an increase of the moisture diffusive resistance, further enhanced for the presence of the oil; in particular, to obtain the same final value of the experimental weight loss in the two EVO tests No. 3 and 4 (Figure 22B, Figure 23B), 16 additional ripening days were required, whereas 3 additional ripening days were enough for the traditional type (Figure 22A, Figure 23A).

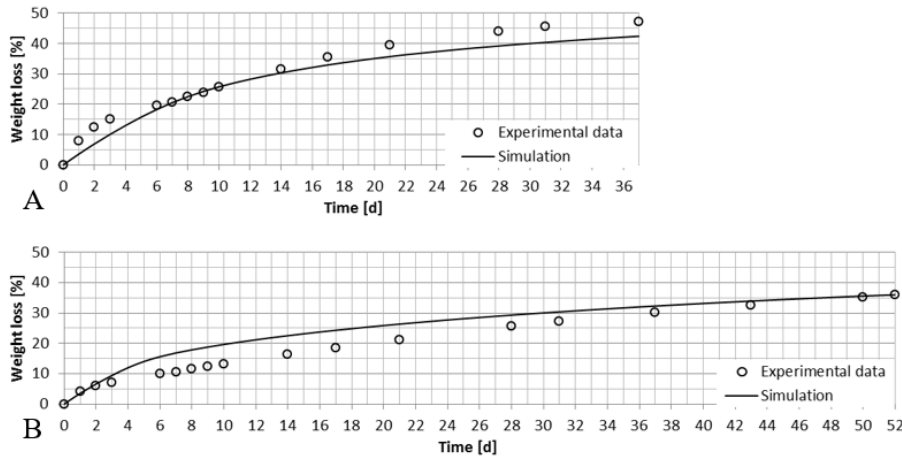


**Figure 22.** Comparison between experimental and predicted sausage weight loss in cylindrical 2D axis-symmetric geometry. SSICA test No. 3 with prediction of shrinking for a) Traditional sausage; b) EVO sausage

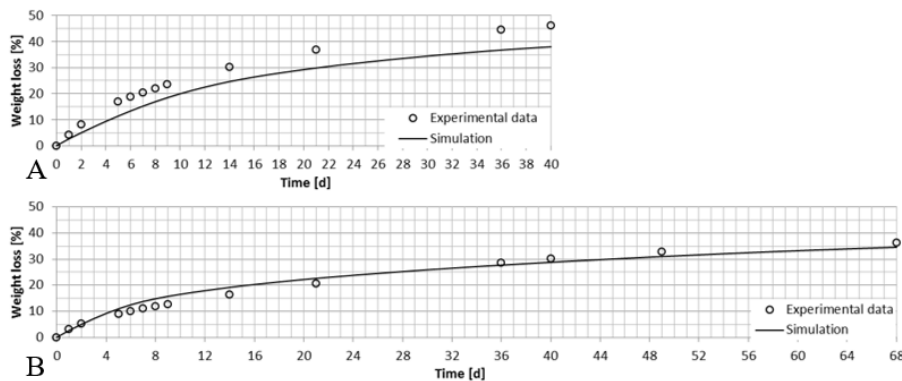


**Figure 23.** Comparison between experimental and predicted sausage weight loss in cylindrical 2D axis-symmetric geometry. SSICA test No. 4 with prediction of shrinking for a) Traditional sausage; b) EVO sausage

## 2.7 Conclusive remarks

A state-of-the-art, flexible, reliable and fast modeling and simulation tool has been successfully developed with COMSOL Multiphysics®4.3 to cope with the issues of sausage irregular shape and shrinking during the ripening process.

The simulation results confirm that the water concentration (or mass fraction) has to be intended as a “distributed parameter” variable in the investigated process.

Vice versa, the sausage temperature should be considered as a “lumped parameter” variable in the investigated mechanism, at least under the conditions of the experimental tests to which the present simulation refers. Actually, from the simulated temperature curves from the center to the surface of the sausage, it appears that the radial temperature profile evolves just in few minutes (i.e., a characteristic time  $\ll 1$  day) after the start-up, then it may change with time, but always remains a flat profile.

The simplification introduced by considering the ripening process to be totally in forced convection (although the chamber has an alternation of natural and forced convection), with average values of curing air conditions over the whole ripening time, provides satisfactory prediction results.

A complication in the sausage shape description does not improve the code prediction of weight loss. On the contrary, the effect of the irregular shape is only a burdening of the computational weight and an increase in the solving time. This is the reason because, for more complex calculation codes, a 2D geometry axi-symmetric was adopted.

There is no doubt that it is more desirable and valuable to have a prediction of the sausage weight loss while taking into account and predicting at the same time the sausage size shrinking. The COMSOL implementation of salami drying as a heterogeneous object in the present model fulfills this task. The simulation with moving mesh provided the opportunity of predicting the shrinkage curves during ripening. The model validation against experimental single sausage shrinkage data proved to be reliable.

However, the advantage provided by such a realistic description of the sausage volume contraction during ripening is partly offset by the inadequacy of the Imre and Kornyei (1990) description of moisture diffusion in a heterogeneous matrix. A problem of availability of diffusivity expressions for the meat matrix was found. Actually, for the EVO sausages no literature correlation exists, therefore the expression of Imre and Kornyei (1990) was artificially corrected.

# Modeling of salami ripening using a heterogeneous approach

## 3.1 Preface

A subsequent development and natural improvement of the mathematical modeling work relies on an innovative description of the sausage as a heterogeneous material, e.g., separately made of lean meat and fat, and as a porous medium. The fat is considered as a discrete inert matter that is dispersed in the meat matrix, while the lean meat is considered as a porous medium in which the transport phenomena of water take place to the outside of the matrix during the ripening process.

To better understand the approximation of the lean part (muscle) to a porous medium, a mention of the muscle structure is necessary.

Lean muscle contains approximately 75% water (Huff-Loneragan et al., 2005). The other main components include protein (approximately 20%), lipids or fat (approximately 5%), carbohydrates (approximately 1%) and vitamins and minerals (often represented as ash in elemental analysis, approximately 1%). The majority of water in muscle is held within the structure of the muscle and muscle cells (Figure 24, Pearce, 2011).

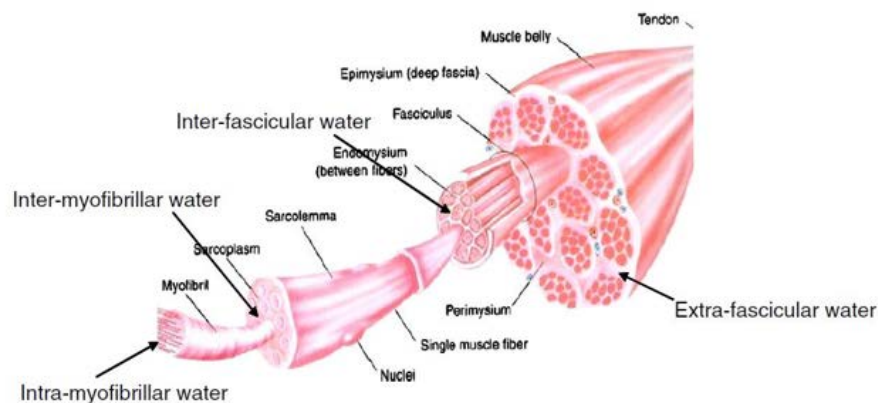


**Figure 24.** The muscle split into components with fibers and the locations of muscle water compartments (Pearce, 2011)

By definition, *bound* water is water that exists in the vicinity of non-aqueous constituents (like proteins) and has reduced mobility, i.e., does not

easily move to other compartments. This bound water only makes up less than a tenth of the total water in muscle (Huff-Lonergan et al., 2005).

Another fraction of water that can be found in muscle is the *entrapped* water. The water molecules in this fraction may be held either by steric (space) effects and/or by attraction to the bound water. This water is held within the structure of the muscle, but is not bound *per se* to protein. In early postmortem tissue, this water does not flow freely from the tissue, yet it can be removed by drying, whereas it can be easily converted to ice during freezing. Entrapped water is most affected by the rigor process and the conversion of muscle to meat. Upon alteration of muscle cell structure and lowering of the pH this water can also eventually escape as purge (Huff-Lonergan et al., 2005).

*Free water* is water whose flow from the tissue is unimpeded. Weak surface forces mainly hold this fraction of water in meat (Huff-Lonergan et al., 2005).

Based on the muscle fiber structure and the above considerations on internal water content, the lean muscle can be considered a porous matrix with a tube bundle structure (Figure 25, Da-Wen Sun et al., 2002).

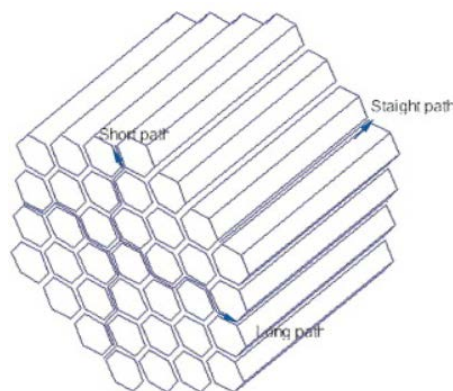


**Figure 25.** Schematic illustration of a hexagonal system as an approximation of the fiber structure of meat (Da-Wen Sun et al., 2002)

### 3.2 Experimental activities

To give greater validity to the porous media approach for the sausages ripening, the structure and water content of a lean meat matrix were experimentally investigated. A sample of the *longissimus dorsi* muscle was taken as representative of pork lean meat used to make salami.

The water content was experimentally evaluated by cutting the *longissimus dorsi* sample in cubes of 10 mm side (Figure 26A) and putting them in a stove at 105 °C for 24 h. The recorded weight loss as averaged over a number of 10 samples yielded the water content, i.e., 74 % wt. This latter is practically the same value reported in literature, i.e., 75% w/w (Huff-Lonergan et al., 2005).

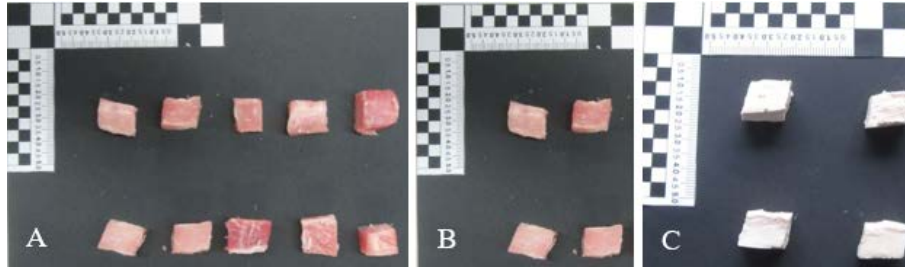


**Figure 26.** Pictures of meat samples cut as cubes of about 10 mm side: A) Fresh cut, B) Frozen, C) Freeze-dried

Then the porosity of the meat matrix was evaluated, following a pre-treatment which did not induce shrinkage of the matrix during the dehydration. After keeping the meat in the freezer @  $-20\text{ }^{\circ}\text{C}$  for 24 h, it was gently cut in order to realize cubic samples of 10 mm side as uniformly as possible (Figure 26B). The cubes were subjected to a two-stage freeze-drying process: primary freeze-drying @  $5\text{ }^{\circ}\text{C}$  for 24 h and secondary freeze-drying @  $35\text{ }^{\circ}\text{C}$  for 7 h, yielding the samples shown in Figure 26C.

The porosity of the samples was evaluated with the Hg penetration technique using the “PASCAL 140” and “PASCAL 240” Thermo Finnigan instruments. This yielded a value of  $\varepsilon = 0.78$ , which well corresponds to the volume of water lost after freeze-drying under the reasonable assumption that all the porosity of the matrix was filled with water.

SEM (scanning electron microscopy) images were taken of freeze-dried samples of Figure 26C. These samples were cut in liquid nitrogen along an orthogonal plane to the direction of the muscle fibers. From the SEM images a “shell and tube” structure emerges (Figure 27), which supports the tube bundle structure representation (Figure 25) and the recourse to the porous media approach to study the lean meat matrices.

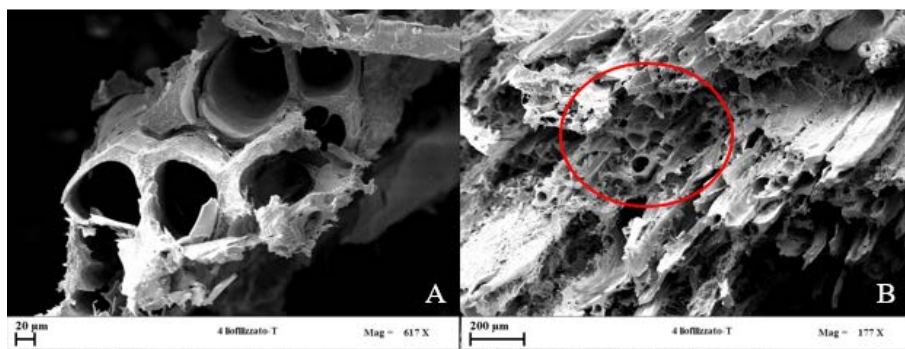


**Figure 27.** SEM freeze-died samples in 20  $\mu\text{m}$  scale (A) and in 200  $\mu\text{m}$  scale (B)

### 3.3 Mathematical modeling

The mathematical model considers the sausage as a heterogeneous, but still isotropic material, with no distinction between the inner part and the casing. Therefore, the sausage is a two-phase material consisting of a fatty part regularly dispersed in a porous matrix (lean meat) in which the moisture transport phenomena take place (the fat as inert and the lean meat as a porous medium). The water present in the whole sausage is assumed present in the lean meat only. The model of the porous system assumes small pores ( $\approx 100 \mu\text{m}$ ), weak evaporation and a capillary pressure formulation (Figure 28, Datta, 2007).

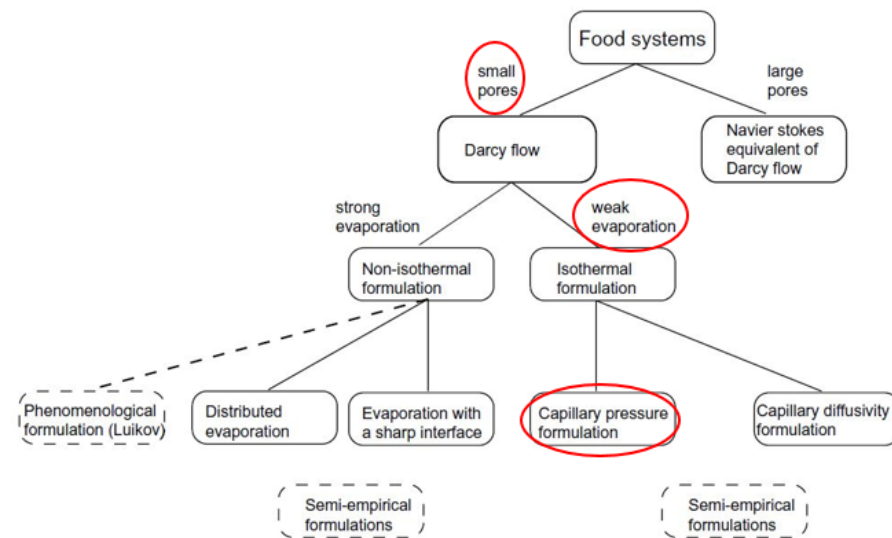


**Figure 28.** Schematic showing the various porous media formulations and their interrelations in the context of food processes (Datta, 2007)

Water concentration is a distributed parameter where the mass flux of liquid for moisture transfer in porous media generally is (Datta, 2007):

$$n_i^{press, cap} = \rho_l \underbrace{u}_{\text{velocity due to gas pressure}} - \underbrace{D_c \frac{\partial c_l}{\partial s}}_{\text{capillary diffusion conc. effect}} - \underbrace{D_T \frac{\partial T}{\partial s}}_{\text{capillary diffusion temp. effect}} \quad (5)$$

The salami ripening process does not present internal evaporation phenomena. Furthermore, the temperature effects are negligible since the initial thermal transient is quite limited (i.e., the length of the drying phase is by far lower than that of the ripening phase) and the temperature difference between product and curing air is in the order of  $0.1 \text{ }^\circ\text{C}$  during the ripening phase.

For these reasons, the contributions due to the gas velocity and temperature in equation (5) are negligible and the governing equation is (Datta, 2007):

$$\frac{\partial c_w}{\partial t} + \nabla \left( -\rho_w \frac{k_w}{\mu_w} \nabla (P - p_c) \right) = \dot{I} \quad (6)$$

where:

$c_w$ = water mass concentration (kg/m<sup>3</sup>);

$t$ = time;

$\rho_w$ = water density (kg/m<sup>3</sup>);

$k_w$ = water permeability (m<sup>2</sup>);

$\mu_w$ = water viscosity (kg/m s);

$P$ = pressure (Pa);

$p_c$ = liquid pressure (Pa);

$\dot{I}$ = rate of evaporation (kg/m<sup>3</sup>s).

In the case of a very wet material with no significant evaporation (region “A” in Figure 29, Saravacos, 2001) because of a low temperature, it happens that  $p_c \gg P$  and  $\dot{I}=0$ , so the previous equation simplifies to the following one:

$$\frac{\partial c_w}{\partial t} + \nabla \left( \rho_w \frac{k_w}{\mu_w} \nabla (p_c) \right) = 0 \quad (7)$$

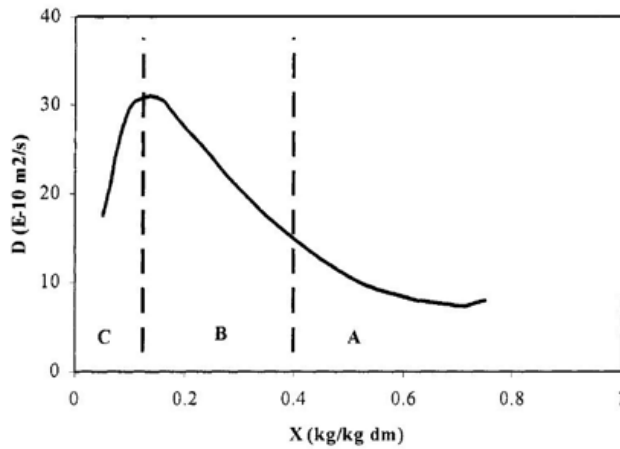


**Figure 29.** Prevailing mechanisms of water transport in porous food materials. A, liquid diffusion and capillary flow; B, vapor diffusion; C, desorption of sorbed water (Saravacos, 2001)

Finally, according to the discussion in Datta (2007), a water concentration in the capillary system is preferred to the capillary pressure formulation, and a capillary diffusivity of liquid water is introduced in place of water permeability. This yields the model adopted here (equation 7):

$$\frac{\partial c_w}{\partial t} - \nabla (D_w \nabla c_w) = 0 \quad (7)$$

I.C.:  $X(0, r) = X_0$

$$B. C. : \begin{cases} \left(\frac{\partial X}{\partial r}\right)_{r=0} = 0 \\ -\rho_{ds} D_w \left(\frac{\partial X}{\partial r}\right)_{r=R} = N_R M_w \end{cases}$$

where:

$c_w$ = water concentration in the capillary system (kg/m<sup>3</sup>);

$D_w$ = capillary diffusivity (m<sup>2</sup>/s);

$X=f(c_w)$ , moisture content on dry basis;

$t$ = time;

$r$ = radius;

$\rho_{ds}$ = dry solid density;

$M_w$ = water molar weight;

$$N_R = k_c \left[ \frac{a_{we}(X(R, t)) \cdot p^*(T(t))}{\mathfrak{R}T(t)} - \frac{RH \cdot p^*(T_a)}{\mathfrak{R}T_a} \right];$$

$N_R$ = mass flux;

$k_c$ = mass transfer coefficient (m/s);

$a_{we}$ = equilibrium water activity on the surface;

$p^*$ = water vapor pressure;

$\mathfrak{R}$ = gas constant;

$RH$ = air relative humidity;

$T_a$ = air temperature.

In very wet materials as the lean meat in a fresh sausage, the capillary diffusivity  $D_w$  is equal to effective diffusivity  $D_e$  because the vapor diffusion is insignificant at the typical ripening temperatures (Datta, 2007).

However, the effective diffusion coefficient depends on the local water content (Saravacos, 2001). In this modeling work, the expression of the effective diffusivity by Saravacos (2001) was used:

$$D = \frac{1}{1+X} D_0 \exp \left[ -\frac{E_0}{R} \left( \frac{1}{T} - \frac{1}{T_r} \right) \right] + \frac{X}{1+X} D_i \exp \left[ -\frac{E_i}{R} \left( \frac{1}{T} - \frac{1}{T_r} \right) \right] \quad (8)$$

where:

$D$ = effective moisture diffusivity (m<sup>2</sup>/s);

$T$ = temperature;

$T_r$ = 60°C, reference temperature;

$R$ = 0.0083143 (kJ/mol K), ideal gas constant;

$X$ = moisture content of lean meat (kg/kg<sub>db</sub>);

$D_0$ = diffusivity @  $X=0$ ,  $T=T$  (m<sup>2</sup>/s);

$D_i$ = diffusivity @  $X=\infty$ ,  $T=T_r$  (m<sup>2</sup>/s);

$E_0$ = activation energy for diffusion @  $X=0$  (kJ/mol);

$E_i$ = activation energy for diffusion @  $X=\infty$  (kJ/mol).

Finally, based on the above discussions about the temperature effects, the water capillary transport, and hence the salami, is considered fully isothermal and no energy balance equation is added to the above water mass balance (Equation 7).

### 3.4 Comsol Multiphysics® code implementation

The COMSOL Multiphysics® 4.3b software was chosen as the modeling, simulation and graphical environment to handle the issue of the porous media approach during drying.

To study the salami as a heterogeneous material, a matrix composed of fat and meat has to be described. The porous medium approach makes it possible to consider the fat as inert and the lean meat as a porous medium in which the water transport takes place.

The “Transport in porous media” physics, adapted to Datta (2007) model, was invoked to develop a code in COMSOL Multiphysics®. The governing equation, i.e., the water mass balance, expressed in terms of Partial Differential Equations (PDEs) with boundary and initial conditions, was solved by COMSOL by means of the Finite Element Methods (FEM). The initial and boundary conditions described in mathematical model were simply introduced in the adopted physics.

The grains that form the sausage paste (both fat and meat) introduce a discontinuity in the solid matrix and represent obstacles to the moisture transport to the outside (Figure 30). This further resistance was dealt with the introduction a tortuosity factor liable to lower the moisture diffusion rate:

$$D_{eff} = \frac{1}{\tau} D \quad (9)$$

where:

$$\tau = \frac{\text{Real path of water from A to B}}{\text{Distance from A to B}}, \text{ tortuosity.}$$

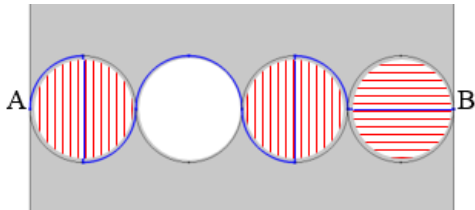


**Figure 30.** Schematic representation of the water flow path in the minced mix in radial direction (from left to right). The meat beads (parallel line pattern) and the fat beads (solid fill) have the same size ( $d = 5 \text{ mm}$ )

A tortuosity factor  $\tau \approx 2$  was simply calculated from a reasonable geometric representation of the water flow path in radial direction inside the minced mix made of meat and fat beads (Figure 30).

Firstly, a 3D calculation scheme was attempted in COMSOL Multiphysics®, but the code crashed on the available MS Windows workstation with Intel® Core™ i7-6700HQ processor, 2.60 GHz clock rate and 32 GB RAM. To limit the load in calculation resources and the time

required for the model resolution, a perfect cylindrical 2D axi-symmetric geometry was chosen as the domain for implementation.

The volume to be attributed to the fat phase was calculated from the original recipe of the Dodaro manufacturer (Table 2:  $\text{mass}_{\text{lean meat}}/\text{mass}_{\text{fat}} = 80/20$  in the reference recipe) and suitably assigned to the cylindrical domain.

In more details, the fat was evenly divided in toroids with a diameter of 5 mm (i.e., the same size of the fat grains in the original recipe) placed inside the cylindrical matrix. The fat phase was not assigned in the form of spheres because this would have required a 3D modeling geometry with a much heavier computational burden.

The used mesh for the simulation is of the type Free triangular with calibrated dimension for General physics Finer (Figure 31).

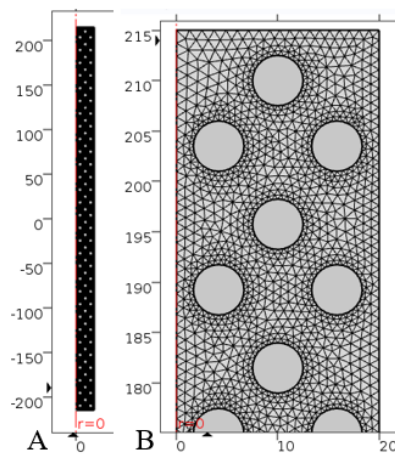


**Figure 31.** Cylindrical 2D axi-symmetric mesh (A) and its zoom (B) in heterogeneous domain

Properties of the built-in materials in the software were not used, but all the characteristics of the salami were implemented in Parameters in Global definitions (if parameters) or in Variables in Definitions (if variables were depending on the moisture content).

An important change with respect to the implementation of the previous homogeneous model is the expression of the absolute local humidity in the Definitions/Variables branch. It is still on dry basis, but must not include the fat content, for this reason it is:

$$X_a = \frac{m_w}{m_t - m_w - m_{fat}} \quad (10)$$

where:

$X_a$ = local moisture content on dry basis;

$m_w$ = water mass;

$m_t$ = sausage weight;

$m_{fat}$ = fat mass.

The model was validated against the results coming from the Dodaro ripening test. So, as input to the code, the data related to the ripening of the non-spicy Dodaro sausage, i.e., the initial properties of the fresh sausage and the ripening air conditions, were used.

**Table 16.** Code data input with porous media model for the Dodaro sausage ripening

Name	Value	Description
$T_0=T_{air}=T$	288.05 K	Air and salami temperature
$X_{r_0}$	0.67	Initial salami moisture fraction
$m_t$	497 g	Initial sausage weight
L	430 mm	Sausage length
D	40 mm	Sausage diameter
RH	0.68	Air relative humidity
$k_{oswin}$	10.8e-2	K Oswin constant
$n_{oswin}$	0.43	n Oswin constant
u	0.2 m/s	Average velocity of air stream “bathing” the products
Duration	24 d	Overall length of the ripening test
Step	1 d	Calculation step
$m_{fat}$	0.2 $m_t$	Fat mass
$m_{meat}$	0.8 $m_t$	Lean meat mass
$D_{fat}$	5 mm	Fat grain diameter

The other parameters depending on temperature and water concentration were literature correlations (Perry et al., 1998).

The equation used for water diffusivity in the porous media is the eq. (8). However, in literature values of the diffusivities  $D_0$ ,  $D_i$  and of the activation energies  $E_0$ ,  $E_i$  for the sausages are not available; for this reason, a rough estimation for them is here taken from the case of a well investigated material, i.e., potato (Saravacos, 2001):

**Table 17.** Diffusivity parameters of the potato from literature

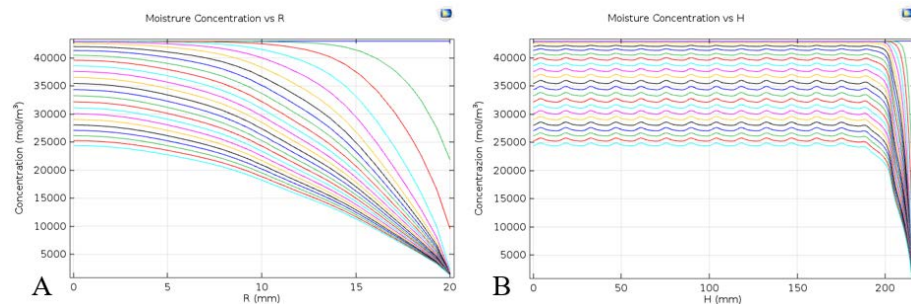
Name	Value
$D_0$	$4.31 \cdot 10^{-10} \text{ m}^2/\text{s}$
$D_i$	$1.57 \cdot 10^{-9} \text{ m}^2/\text{s}$
$E_0$	76.9 kJ/mol
$E_i$	44.7 kJ/mol

The development of the codes and the simulation runs have been carried out with a MS Windows workstation based on the Intel® Core™ i7-6700HQ processor with 2.60 GHz clock rate and 32 GB RAM.

### 3.5 Simulation results

The simulation work has been started by taking as a reference the previously mentioned ripening test carried out at Dodaro SpA. Drying in a unique phase was considered under forced air circulation, that is a condition corresponding to values of air temperature, relative humidity and velocity as averaged over the whole duration of the ripening test, i.e., 24 days.

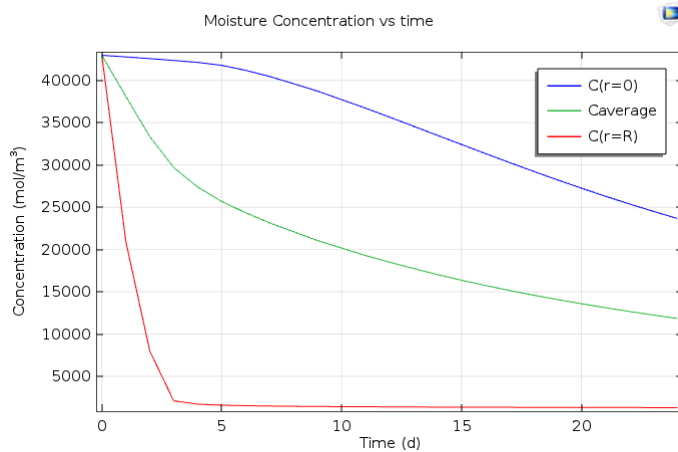
The Figure 32 is example of the way the profile of water concentration can be graphically reported as a function of time from the center to the surface of the sausage. In particular, Figure 32 shows how the water concentration profile is gradually lowered day by day both along radial (Figure 32A) and axial (Figure 32B) position. The diagram in Figure 32A refers to an axial position in the mesh domain that is free of fat thoruses. The Figure 32B shows how the presence of inert fat elements placed in the calculation domain has an effect on the moisture concentration profiles, by causing a characteristic series of small oscillations along the vertical axis.



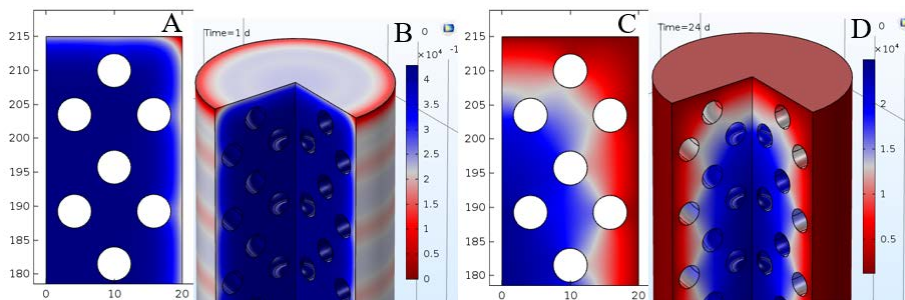
**Figure 32.** Water concentration ( $\text{mol/m}^3$ ) profile as a function of the radial position ( $R$ ) (A) and the axial position ( $H$ ) (B) parametrically in the ripening day

Figure 33 shows another post-processing graph: the most significant water average concentration profiles on the axis  $C_{r=0}$ , volume-averaged  $C_{\text{average}}$  and on the wall  $C_{r=R}$  as a function of time during the whole ripening. The wall moisture concentration falls very quickly according to the involved transport phenomena; instead the concentration on the axis shows a change in concavity and a slower decrease in concentration according to the ripening process.

Figure 34 show the color plots of the water concentration ( $\text{mol/m}^3$ ) in the sausage, precisely at both the time extremes of the ripening test, that is the end of day 1 (Figure 34A and B) and that of day 24 ((Figure 34C and D). In the 2D and 3D representation the effect of the inert fat phase is well shown on the moisture concentration profile.



**Figure 33.** *The most significant water concentration profiles during the ripening time*



**Figure 34.** *Zoom of plot of the water concentration ( $\text{mol}/\text{m}^3$ ) in the sausage at day 1 in 2D (A) and 3D (B) view and at the day 24 in 2D (C) and 3D (D) view*

### 3.6 Comparison between predicted and experimental results

The code validation has been pursued thanks to the results of the previously mentioned ripening test carried out at Dodaro SpA.

Figure 35 reports the comparison between experimental and predicted single sausage weight loss obtained according to a simulation as a homogeneous material and the present simulation as a heterogeneous material (porous medium). The experimental data are provided in 2 different sets for Inoculated (I) and Non-Inoculated sausages (NI), each averaged over several samples.

All in all, the prediction of the sausage weight loss turns out satisfactory. The simulated curves appear close enough to the experimental data in spite of the underlying assumption of a unique value (averaged conditions) of air temperature, relative humidity and velocity throughout the whole duration of

the test. One noticeable difference is seen in the early days of ripening in the simulation based on the porous media approach compared to experimental data. This is probably due to the approximation induced by the expression adopted for the effective diffusivity (as a function of the water concentration) that uses some literature parameters not specific for the sausage. In the following days of ripening, both models have a good prediction of weight loss compared to the experimental data.

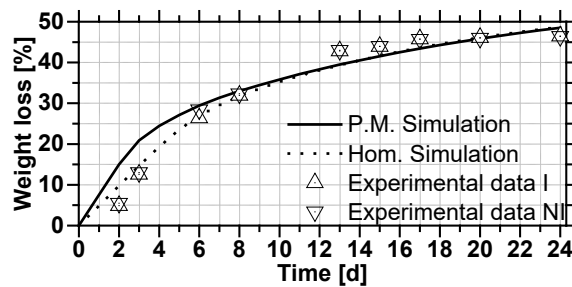


**Figure 35.** Comparison between experimental and predicted sausage weight loss in heterogeneous (porous medium) and homogeneous model

Figure 36 shows the trends of the water content for the different simulations compared to the experimental data. Also here there was a discrepancy in the first days of ripening with a good prediction in the following days for the reasons mentioned above.

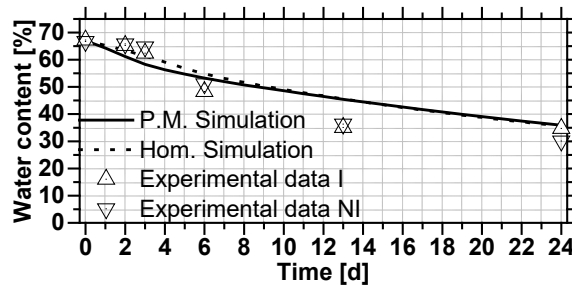


**Figure 36.** Comparison between experimental and predicted values of the average sausage water content in heterogeneous (porous medium) and homogeneous model

The use of “moving mesh” for a simulation with the porous media approach turned out to be too heavy. However, it was still possible to estimate the diameter reduction by means of the Feyissa (2009) equation as a post-processing result at each calculation time.

Figure 37 shows an excellent agreement of the new heterogeneous model with the experimental data and an improvement with respect to the previous homogeneous model in the prediction of the % diameter shrinkage.

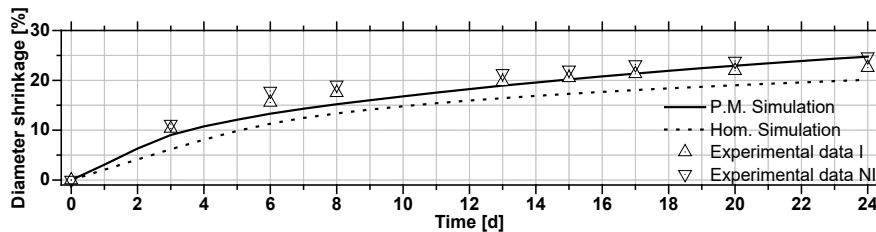


**Figure 37.** Comparison between experimental and predicted diameter shrinkage curves: simulation with the homogeneous model with shrinking and calculation of a diameter reduction with the data of the porous medium

### 3.7 Conclusive remarks

A flexible, reliable and fast modeling and simulation tool has been successfully developed with COMSOL Multiphysics®4.3 to cope with the issue of heterogeneity of the sausage during the ripening process. The present COMSOL code retains the satisfactory prediction performance for the time evolution of the single sausage weight loss and volume-averaged water content.

The simplification introduced by considering the ripening process to be totally in forced convection (although the chamber has an alternation of natural and forced convection) with average values of curing air conditions over the whole ripening time provides satisfactory prediction results. The heterogeneous model allows a definition of the sausage structure much closer to the real salami structure with good predictive results.

The model with porous media approach can be improved by identifying a semi-empirical relationship for the effective diffusivity in the porous medium, going beyond the approximation induced by the absence of literature data.



# **Modeling of meat drying as a porous medium based on ad hoc experimental apparatus and procedure**

## **4.1 Experimental**

As discussed in the previous chapters, a lack and an inadequateness of literature data was found on moisture diffusivity in the complex matrix, such as the minced mixture of lean meat and fat globules, subject to drying and ripening in the salami production process.

Therefore, a new experimental apparatus and the related procedure were developed to allow the evaluation of moisture diffusivity data in the meat matrix during the drying process and, hence, a trustable correlation providing the dependence of the diffusion coefficient from the local moisture content and temperature.

### ***4.1.1 Apparatus***

The apparatus is a sample holder equipped with a real-time acquisition system that allows i. monitoring the sample weight, ii. measuring the water content in various points of the specimen and iii. measuring temperature and humidity of the environmental air (Figure 38).

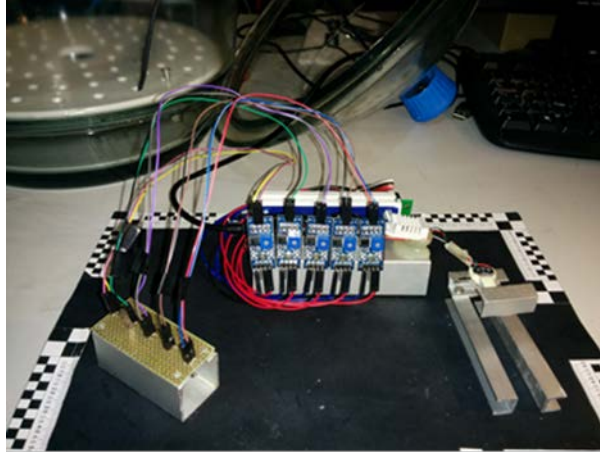


**Figure 38.** *Experimental apparatus with the sample holder and the various sensors*

Data are processed by an Arduino Nano MCU. Therefore, the system consists of:

- 1 MCU Arduino Nano, an open-source hardware, for data acquisition and screen printing in real time (Figure 39). It can be programmed with the Arduino software.

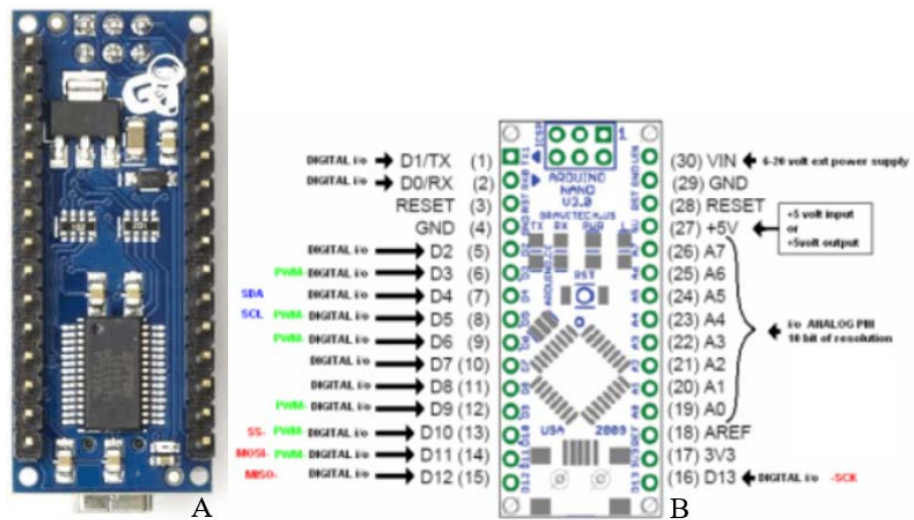


**Figure 39.** *Arduino nano picture (A) and pin input-output configuration (B)*

- 1 Digital-output relative humidity & temperature DHT22 sensor/module (Figure 40A) for monitoring temperature and humidity of the environmental air. The capacitive-type humidity and temperature module/sensor utilizes exclusive digital-signal-collecting-technique and

humidity sensing technology, assuring its reliability and stability. Its sensing elements are connected to an 8-bit single-chip computer.

Measuring range: humidity 0-100% RH; temperature -40~125°C.

- 1 24-bit Analog-to-Digital Converter (ADC) (Figure 40B) for Weigh Scales in order to acquire sample weight. HX711 is a precision 24-bit analog to-digital converter (ADC) designed for weigh scales and industrial control applications to interface directly with a bridge sensor.

Measuring range: 0.000~100.000 g @ -40~85°C.

- 5 high sensitivity moisture sensors (Figure 40C) for measuring the water content in the sample at different points. This moisture sensor uses two probes to pass current through the matrix, originally intended to be a soil, and then it reads that resistance to get the moisture level. Abundant water makes a soil conduct electricity more easily (less resistance), while dry meat conducts electricity poorly (more resistance).

Measuring range: 0-100% moisture mass fraction @ 10~30°C.



**Figure 40.** Picture of DHT22 sensor (A), HX711 load cell (B), moisture sensor (C)

Each type of probe required specific programming with zeroing, calibration, sampling time in C++ language. The code developed for such a purpose is reported in Appendix A for reference.

Each drying test lasted at least 3 days and the sampling time was 1 min (i.e., minimum time indicated in the data sheets of the probes for a stable measurement).

With the PLX-DAQ tool (Figure 41) the data are acquired in real-time at each sampling time by a connected PC and transferred to Microsoft Excel, allowing plotting a graph of the time trends, too.

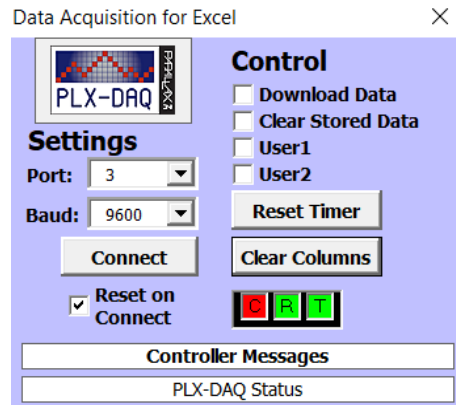


**Figure 41.** *PLX-DAQ pop-up image*

Based on the above description, the experimental apparatus was quite cheap, easy to be assembled and flexible in its operation.

The geometry of the meat sample holder (Figure 42) is designed as a parallelepiped with a length much larger than height, i.e.,  $L$  (60 mm)  $\gg$   $h$  (22 mm), in a way that there are no appreciable variations for water concentration in the sample in the vertical direction and therefore it is possible to sample the concentration variation in the longitudinal direction.

To ensure air circulation, a 5 cm diameter brushless fan at 12 V was used (typical computer cooling fan).



**Figure 42.** *Meat sample holder picture*

#### 4.1.2 Procedure

In this part the material studied, as representative of pork lean meat, is minced *longissimus dorsi* meat.

The experiment is conducted exclusively on such a minced sample of lean meat (without fat as much as possible).

The sample is loaded into the specimen, equipped with humidity sensors and placed on a strain gauge to monitor its weight. After this, the whole system is placed in a humidity-controlled atmosphere dryer; a pre-established air humidity is gathered in the dryer thanks to the presence of a lithium chloride

supersaturation solution, which allows establishing an air humidity equal to 15% RH at ambient temperature. In any case, a sensor monitors the temperature and relative humidity of environmental air.

Many tests were carried out to set up and tune the procedure, including the calibration of the sensors, until reaching a standardization of the experiment duration, set at 72 h (e.g., by observing the deterioration state of the sample and the time in which the weight losses become not appreciable).

Measurement of the sample weight with analytical scale is required at the start of the drying test to calibrate, appropriately, the load cell zero. Then, within the programming language, the *calibration\_factor* value (in Arduino programming) is changed until the load cell produces a weight equal to the measured value on the analytical scale. A separate and independent weight measurement at the end of the drying is done to have a control value.

With subsequent tests, it was decided to sample the voltage values for each sensor of the sample moisture content during drying. The transition from voltage to % mass fraction values occurs by attributing 0% to the voltage value that is returned by the probe not connected to the sample holder and 75% (value of water mass fraction in fresh lean meat) to the voltage value that is provided by the probe just connected to the fresh sample. In this way, a calibration line is constructed for each sensor, with the result of reducing the reading differences between the various sensors.

Two slightly different experimental configurations, i.e., a first one with one moisture exchange surface to environmental air for drying (samples A) and a second one with two surfaces (samples B)(Table 18), were implemented. In any case, each test was performed in triplicate @ 72 h,  $T_{amb}$ , 15% RH, inside the humidity-controlled atmosphere dryer (with lithium chloride supersaturated solution).

**Table 18.** *Experimental data for 1 free surface samples (A) and 2 free surfaces samples (B)*

Sample	Image <sub>IN</sub>	Weight <sub>IN</sub> [g]	Image <sub>OUT</sub>	Weight <sub>OUT</sub> [g]
A1		25.904		19.327
A2		31.734		24.263
A3		31.854		26.473
B1		32.022		23.912
B2		31.389		24.096
B3		32.579		24.16

#### 4.1.3 Results

First of all, the experiments set @ 72 h,  $T_{amb}$ , 15% RH allowed to sample weight loss throughout the time. They are reported in Table 19 (samples A) and Table 20 (samples B) for the configuration with one and two moisture exchange surfaces, respectively.

**Table 19.** *Weight loss data log for the triplicated experiment with 1 exchange surface (A)*

Time [h]	Weight loss A1 [%]	Weight loss A2 [%]	Weight loss A3 [%]	Average [%]	Std deviation
0	0.000	0.000	0.000	0.000	0.000
1	0.000	0.396	0.693	0.363	0.283
2	0.600	0.402	1.012	0.671	0.254
3	1.292	0.464	1.202	0.986	0.371
4	1.892	0.658	1.391	1.314	0.507
5	2.491	0.897	1.625	1.671	0.652
6	3.014	1.162	1.878	2.018	0.762
7	3.441	1.447	2.119	2.335	0.828
8	3.840	1.715	2.346	2.634	0.891
9	4.194	1.967	2.552	2.904	0.943
10	4.509	2.203	2.745	3.153	0.984
11	5.095	2.427	2.928	3.483	1.158
12	5.324	2.647	3.128	3.699	1.166
13	5.527	2.899	3.292	3.906	1.157
14	5.702	3.138	3.482	4.107	1.136
15	5.862	3.384	3.656	4.301	1.110
16	5.999	3.597	3.852	4.483	1.077
17	6.148	3.840	4.060	4.683	1.040
18	6.285	4.070	4.326	4.894	0.989
19	6.464	4.283	4.566	5.105	0.968
20	6.628	4.471	4.804	5.301	0.948
21	6.811	4.707	5.060	5.526	0.920
22	6.948	4.914	5.370	5.744	0.872
23	7.097	5.127	5.645	5.956	0.834
24	7.249	5.331	5.951	6.177	0.799
25	7.429	5.548	6.290	6.422	0.774
26	7.627	5.768	6.600	6.665	0.761
27	7.780	5.987	6.888	6.885	0.732
28	7.901	6.201	7.147	7.083	0.696
29	8.019	6.385	7.412	7.272	0.674
30	8.129	6.570	7.646	7.448	0.652
31	8.236	6.790	7.852	7.626	0.612
32	8.338	6.961	8.020	7.773	0.589
33	8.464	7.155	8.168	7.929	0.560
34	8.582	7.339	8.298	8.073	0.532
35	8.661	7.498	8.428	8.195	0.502
36	8.833	7.682	8.582	8.366	0.494
37	8.974	7.841	8.715	8.510	0.485
38	9.084	8.002	8.854	8.647	0.465
39	9.167	8.183	8.971	8.774	0.425

Time [h]	Weight loss A1 [%]	Weight loss A2 [%]	Weight loss A3 [%]	Average [%]	Std deviation
40	9.254	8.332	9.114	8.900	0.406
41	9.372	8.310	9.250	8.977	0.474
42	9.470	8.462	9.389	9.107	0.457
43	9.561	8.617	9.544	9.241	0.441
44	9.641	8.763	9.664	9.356	0.419
45	9.759	8.915	9.809	9.494	0.410
46	9.857	9.070	9.930	9.619	0.389
47	9.987	9.212	10.075	9.758	0.387
48	10.120	9.351	10.217	9.896	0.387
49	10.234	9.507	10.347	10.029	0.372
50	10.363	9.649	10.489	10.167	0.370
51	10.473	9.775	10.606	10.285	0.365
52	10.572	9.914	10.755	10.414	0.361
53	10.690	10.066	10.888	10.548	0.350
54	10.758	10.199	11.024	10.660	0.344
55	10.841	10.341	11.153	10.778	0.335
56	10.916	10.477	11.286	10.893	0.331
57	11.003	10.616	11.422	11.014	0.329
58	11.091	10.736	11.561	11.129	0.338
59	11.193	10.878	11.688	11.253	0.333
60	11.249	11.011	11.808	11.356	0.334
61	11.333	11.163	11.938	11.478	0.333
62	11.397	11.276	12.048	11.574	0.339
63	11.457	11.418	12.191	11.689	0.355
64	11.548	11.560	12.320	11.809	0.361
65	11.608	11.667	12.510	11.928	0.412
66	11.726	11.774	12.633	12.044	0.417
67	11.809	11.916	12.747	12.157	0.419
68	11.865	12.062	12.880	12.269	0.439
69	11.941	12.159	12.981	12.360	0.448
70	12.013	12.262	13.114	12.463	0.472
71	12.123	12.385	13.234	12.581	0.474
72	12.202	12.524	13.383	12.703	0.498

**Table 20.** *Weight loss data log for the triplicated experiment with 2 exchange surface (B)*

Time [h]	Weight loss B1 [%]	Weight loss B2 [%]	Weight loss B3 [%]	Average [%]	Std deviation
0	0.000	0.000	0.000	0.000	0.000
1	0.194	3.187	0.520	1.300	1.341
2	0.386	3.099	1.411	1.632	1.119
3	0.896	3.464	1.934	2.098	1.055
4	1.499	3.963	2.408	2.623	1.017
5	2.096	4.502	2.912	3.170	0.999
6	2.677	5.101	3.398	3.725	1.016
7	3.209	5.680	3.897	4.262	1.041
8	3.723	6.232	4.404	4.786	1.059
9	4.207	6.734	4.893	5.278	1.067
10	4.631	7.236	5.339	5.735	1.100
11	4.977	7.694	5.800	6.157	1.137
12	5.372	8.102	6.270	6.581	1.136
13	5.783	8.529	6.728	7.013	1.139
14	6.129	8.959	7.167	7.419	1.169
15	6.562	9.368	7.581	7.837	1.160
16	6.921	9.764	8.042	8.243	1.169
17	7.284	10.144	8.482	8.637	1.173
18	7.669	10.512	8.930	9.037	1.163
19	7.996	10.876	9.326	9.399	1.177
20	8.324	11.229	9.706	9.753	1.186
21	8.686	11.522	10.083	10.097	1.158
22	8.984	11.874	10.472	10.443	1.180
23	9.270	12.161	10.815	10.748	1.181
24	9.568	12.422	11.160	11.050	1.168
25	9.873	12.740	11.512	11.375	1.175
26	10.181	13.036	11.843	11.687	1.171
27	10.512	13.317	12.157	11.995	1.151
28	10.826	13.660	12.444	12.310	1.161
29	11.086	13.997	12.746	12.609	1.192
30	11.426	14.324	12.998	12.916	1.184
31	11.760	14.651	13.272	13.228	1.181
32	12.036	14.904	13.515	13.485	1.171
33	12.003	15.178	13.799	13.660	1.300
34	12.003	15.480	14.051	13.845	1.427
35	12.173	15.823	14.306	14.101	1.497
36	12.372	16.122	14.571	14.355	1.538
37	12.661	16.456	14.808	14.642	1.554
38	12.911	16.743	15.073	14.909	1.568
39	13.171	17.051	15.325	15.182	1.587

Time [h]	Weight loss B1 [%]	Weight loss B2 [%]	Weight loss B3 [%]	Average [%]	Std deviation
40	13.457	17.350	15.590	15.466	1.592
41	13.720	17.622	15.833	15.725	1.595
42	14.012	17.887	16.073	15.990	1.583
43	14.320	18.180	16.312	16.271	1.576
44	14.654	18.438	16.552	16.548	1.545
45	14.974	18.731	16.780	16.828	1.534
46	15.273	18.956	16.998	17.075	1.505
47	15.561	19.018	17.203	17.261	1.412
48	15.754	19.277	17.446	17.492	1.439
49	15.869	19.551	17.711	17.710	1.503
50	15.940	19.682	18.001	17.874	1.530
51	16.210	19.962	18.237	18.136	1.534
52	16.473	20.268	18.418	18.386	1.550
53	16.726	20.536	18.574	18.612	1.556
54	16.963	20.807	18.798	18.856	1.570
55	17.166	21.078	19.013	19.086	1.598
56	17.348	21.321	19.218	19.296	1.623
57	17.486	21.599	19.440	19.508	1.680
58	17.650	21.848	19.642	19.713	1.715
59	17.839	22.091	19.848	19.926	1.737
60	18.077	22.316	20.081	20.158	1.731
61	18.337	22.550	20.290	20.392	1.721
62	18.606	22.793	20.492	20.630	1.712
63	18.853	23.017	20.698	20.856	1.704
64	19.091	23.248	20.922	21.087	1.701
65	19.296	23.482	21.137	21.305	1.713
66	19.524	23.734	21.368	21.542	1.723
67	19.745	23.965	21.558	21.756	1.728
68	19.938	24.174	21.782	21.964	1.734
69	20.047	24.379	21.953	22.126	1.773
70	20.281	24.582	22.150	22.337	1.761
71	20.489	24.800	22.346	22.545	1.765
72	20.704	25.018	22.598	22.774	1.765

The five probes for measuring the water mass fraction allowed determining a dimensionless moisture content (in terms of  $C/C_0$ ) in 5 points of the longitudinal direction of the sample holder. It was decided to take into consideration a new concentration profile in the longitudinal direction just every 24 h, in order to observe appreciable changes in the experimental data.

The results are reported in Table 21 (samples A) and Table 22 (samples B) for the configuration with one and two moisture exchange surfaces, respectively.

**Table 21.** *C/C<sub>0</sub> data log for triplicated 1-moisture exchange surface experiment (A)*

Sample A1				
Longitudinal abscissa [mm]	0 h	24 h	48 h	72 h
5	1.000	1.014	1.014	1.014
15	1.000	0.946	1.014	0.973
30	1.000	1.014	1.000	1.014
45	0.986	0.973	0.973	0.959
55	0.986	0.946	0.932	0.905
Sample A2				
Longitudinal abscissa [mm]	0 h	24 h	48 h	72 h
5	0.999	0.901	0.974	0.889
15	1.000	0.923	0.914	0.883
30	0.995	0.999	0.927	0.897
45	0.998	0.919	0.896	0.969
55	0.997	0.989	0.921	0.847
Sample A3				
Longitudinal abscissa [mm]	0 h	24 h	48 h	72 h
5	0.998	0.893	0.993	0.934
15	0.996	0.719	0.918	0.800
30	1.000	0.826	1.025	0.937
45	0.996	0.761	0.996	1.018
55	0.997	0.781	0.805	0.833
Average				
Longitudinal abscissa [mm]	0 h	24 h	48 h	72 h
5	0.999	0.954	1.013	0.964
15	0.999	0.923	1.015	0.947
30	0.998	0.946	0.984	0.949
45	0.994	0.796	0.860	0.884
55	0.993	0.634	0.620	0.603
Std deviation				
Longitudinal abscissa [mm]	0 h	24 h	48 h	72 h
5	0.001	0.055	0.016	0.051
15	0.002	0.102	0.046	0.071
30	0.002	0.085	0.041	0.049
45	0.005	0.090	0.043	0.026
55	0.005	0.089	0.058	0.031

**Table 22.**  $C/C_0$  data log for triplicated 2-moisture exchange surface experiment (B)

Sample B1				
Longitudinal abscissa [mm]	0 h	24 h	48 h	72 h
5	0.971	0.900	0.878	0.865
15	0.993	0.918	0.949	0.956
30	1.000	0.967	0.952	0.913
45	0.993	0.951	0.918	0.887
55	0.993	0.905	0.809	0.795
Sample B2				
Longitudinal abscissa [mm]	0 h	24 h	48 h	72 h
5	0.990	0.835	0.882	0.660
15	0.991	0.939	0.865	0.811
30	1.000	0.912	0.910	0.858
45	1.000	0.918	0.855	0.919
55	0.991	0.839	0.813	0.810
Sample B3				
Longitudinal abscissa [mm]	0 h	24 h	48 h	72 h
5	1.000	0.827	0.948	0.881
15	1.000	0.956	0.970	0.893
30	1.000	0.920	0.857	0.775
45	1.000	0.932	1.009	0.973
55	1.000	0.958	0.976	0.958
Average				
Longitudinal abscissa [mm]	0 h	24 h	48 h	72 h
5	0.987	0.589	0.623	0.554
15	0.995	0.937	0.928	0.887
30	1.000	0.998	0.970	0.908
45	0.998	0.933	0.927	0.927
55	0.995	0.622	0.598	0.589
Std deviation				
Longitudinal abscissa [mm]	0 h	24 h	48 h	72 h
5	0.012	0.033	0.032	0.100
15	0.004	0.016	0.045	0.060
30	0.000	0.024	0.039	0.057
45	0.003	0.013	0.063	0.036
55	0.004	0.049	0.078	0.074

## 4.2 Mathematical modeling

The mathematical model in this part of work is a porous media approach system with small pores ( $\approx 100 \mu\text{m}$ ), weak evaporation and a capillary pressure formulation (Datta, 2007). Thus, the mathematical model is the one previously shown in eq. (7):

$$\frac{\partial c_w}{\partial t} - \nabla(D_w \nabla c_w) = 0 \quad (11)$$

$$I. C.: @t = 0, c_w = c_0$$

$$B. C.: \begin{cases} @ x \in \Gamma_{NO\ flux}, N_w = 0, & \forall t > 0 \\ @ x \in \Gamma_{flux}, N_w = N_R, & \forall t > 0 \end{cases}$$

where:

$c_w$ = water concentration in the capillary system ( $\text{kg}/\text{m}^3$ ),  $c_w=f(X)$ ;

$D_w$ = capillary diffusivity ( $\text{m}^2/\text{s}$ );

$X=f(c_w)$ , moisture content on dry basis;

$t$ = time;

$N_w$ = water interface flux;

$N_R$ = water interface flux described in eq. (1);

$\Gamma_{flux}$ = boundary where the mass transfer take place;

$\Gamma_{NO\ flux}$ = boundary where the mass transfer does not take place.

For the reason explained above, inert fat as dispersed in the meat matrix was not present and hence not considered. Therefore, the model now represents a homogeneous material, although as a porous medium.

As highlighted in the previous chapters, due to a lack of literature data for the expression of diffusivity in the meat matrix, it appeared convenient, as a first attempt to the simulation work, to adopt a simple equation describing the moisture diffusion in swordfish tissue (Zogzas, 2013):

$$D_w = 9 \cdot 10^{-11} + 1.6 \cdot 10^{-10} X \quad (12)$$

where:

$D_w$ = effective diffusivity ( $\text{m}^2/\text{s}$ );

$X$ = moisture content on dry basis;

It has the advantage of being a linear diffusivity correlation with the water content.

## 4.3 Comsol Multiphysics® code implementation

The COMSOL Multiphysics® 4.3b software was chosen as the modeling, simulation and graphical environment.

### 4.3.1 Drying

The porous medium approach makes it possible to consider the lean meat as a porous medium in which the water transport takes place.

The “Transport in porous media” physics, adapted to Datta (2007) model, was adopted to develop a code in COMSOL Multiphysics®. The governing equations, i.e., the water mass balance, expressed in terms of Partial Differential Equations (PDEs) with their boundary and initial condition, were solved by COMSOL by means of the Finite Element Methods (FEM).

The initial and boundary conditions described in mathematical model were applied to the adopted physics.

The sample holder was built with a simple shape in order to choose a 3D Geometry (Figure 43A) as the domain for implementation. The energy balance was neglected because the drying experiment was carried out at ambient temperature in an isothermal manner.

The used mesh for the simulation is of the type Free Tetrahedral with calibrated dimension for General physics Extremely fine (Figure 43B).

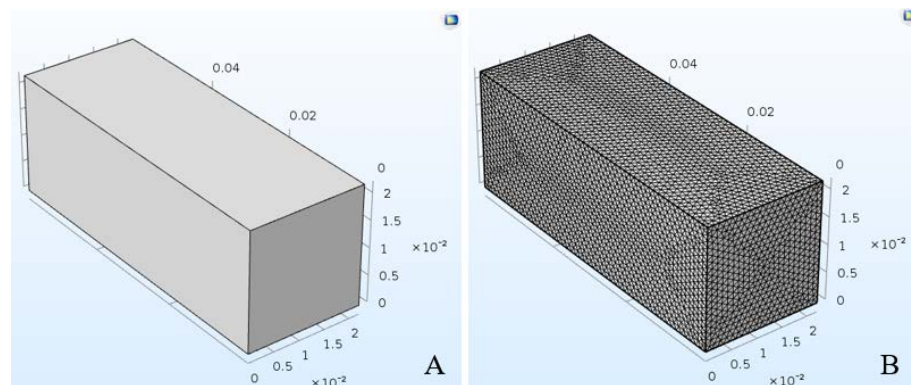


**Figure 43.** Specimen 3D geometry (A) and Mesh (B)

Properties of the built-in materials in the software were not used, but all the characteristics of the lean meat were implemented in Parameters in Global definitions (if parameters) or in Variables in Definitions (if variables depending on the moisture content).

Running the code requires as input data the initial properties of the fresh minced lean meat (commercial *longissimus dorsi* pork meat) and the drying air conditions. So, as input to the model, the data related to experimental drying test were used:

**Table 23.** Code data input with porous media model for the experimental drying conditions

Name	Value	Description
$T_0=T_{\text{air}}=T$	303 K	Air and meat temperature
$X_{r0}$	0.75	Initial meat moisture fraction
$m_t$	31.997 g	Initial meat weight
$L_{\text{sample}}$	60 mm	Specimen length
$B_{\text{sample}}$	22 mm	Specimen height
RH	0.15	Air relative humidity
$k_{\text{oswin}}$	10.8e-2	K Oswin constant
$n_{\text{oswin}}$	0.43	n Oswin constant
$u$	0.2 m/s	Air velocity
Duration	3 d	Drying duration
Step	0.1 d	Calculation step

The other parameters with dependencies from temperature and water concentration are literature correlations (Perry et al., 1998).

The correlation for the water diffusivity in the porous medium is the Zogzas, (2013) eq. (12).

The mathematical model implementation requires to choose 1 or 2 boundary surface  $\Gamma_{\text{flux},s}$ , according to the two types of experimental configurations, i.e., the first one with one moisture exchange surface for drying (samples A) and the second one with two surfaces (samples B).

#### 4.3.2 Optimization procedure for diffusivity parameter estimation

Afterwards, with the available experimental data of moisture concentration and weight loss, a parameter optimization idea was conceived and code was implemented in COMSOL to determine the optimal parameters for a more reliable correlation able to express moisture diffusivity in lean meat during drying.

For mass transfer, the “Transport in porous media” physics, adapted to Datta (2007) model, was adopted to develop a code in COMSOL Multiphysics<sup>®</sup>. The governing equations, with their boundary and initial condition, were solved by COMSOL by means of the Finite Element Methods (FEM). The initial and boundary conditions described in mathematical model were applied to the adopted physics.

The shape of the sample holder with  $L$  (60 mm)  $\gg$   $h$  (22 mm) allowed having appreciable concentration variations only in the longitudinal direction ( $x$ ). In this way, it was possible to choose a 1D geometry in the  $L$  direction for the mass transfer phenomena, to make the model computations less time-consuming in COMSOL.

Also in this case, the energy balance was neglected because the drying experiment is carried out at environment temperature in isothermal manner.

With this simplification, it was possible to add to the calculation code the “Optimization” physics, which is built in COMSOL. The objective was to determine the optimal values of the parameters appearing as coefficient in two expressions of water diffusivity in a food-like porous medium taken from literature. In particular, the first one is the previously mentioned eq. (8) for effective diffusivity (Saravacos, 2001): in this case, the optimal values of the parameters  $D_0$ ,  $D_i$ ,  $E_0$ ,  $E_i$  were determined. The second one is the semi-empirical formulation of capillary diffusivity (Datta, 2007):

$$D_w = A \exp[-B + C \cdot M] \quad (13)$$

where:

$D_w$ = capillary diffusivity ( $m^2/s$ );

$M$ = moisture content of lean meat ( $kg/kg_{ab}$ ).

Where the optimal parameters to be determined are  $A$ ,  $B$ ,  $C$ .

The implementation of this physics involves the use of two types of data:

- global experimental data sets (weight loss) on the domain throughout the whole test-time in the option “Global Least-Squares Objective”.
- local experimental data sets (water concentration profile) on the domain at fixed drying times 0 h, 24 h, 48 h, 72 h in the option “Least-Squares Objective”.

This new physics also required the inclusion of an "Optimization" item in the "Study" option in which the user chooses the method to solve the optimization calculation with the experimental data: in this work, the Levenberg–Marquardt Algorithm is chosen. This latter concerned the minimization of an objective function defined as the sum over time of the squared errors between the simulated and experimental results, firstly for a macroscopic variable such as the sample weight loss, secondly for a variable changing in the spatial domain such as the water concentration.

The used Mesh for the simulation is of the type with calibrated dimension for General physics Extremely fine.

Properties of the built-in materials in the software were not used, but all the characteristics of the lean meat were implemented in Parameters in Global definitions (if parameters) or in Variables in Definitions (if variables depending on the moisture content).

Running the code required as input data the initial properties of the fresh minced lean meat (commercial *longissimus dorsi* pork meat), the drying air conditions and the starting values of the parameters to be optimized.

So, as input to the model, the data related to experimental drying were used:

**Table 24.** Code data input with porous media model for the 1D experimental drying case

Name	Value	Description
$T_0=T_{\text{air}}=T$	303 K	Air and meat temperature
$X_{r0}$	0.75	Initial meat moisture fraction
$m_t$	31.997 g	Initial meat weight
$L_{\text{sample}}$	60 mm	Specimen length
RH	0.15	Air relative humidity
$k_{\text{oswin}}$	10.8e-2	K Oswin constant
$n_{\text{oswin}}$	0.43	n Oswin constant
$u$	0.2 m/s	Air velocity
Duration	3 d	Drying duration
Step	0.1 d	Calculation step

The calculation code, which optimizes the effective diffusivity expressed by eq (8), has the parameters of the potato (see the previous chapter) as starting values (Saravacos, 2001):

**Table 25.** Starting parameters in optimization of effective diffusivity

Name	Value
$D_0$	$4.31 \cdot 10^{-10} \text{ m}^2/\text{s}$
$D_i$	$1.57 \cdot 10^{-9} \text{ m}^2/\text{s}$
$E_0$	76.9 kJ/mol
$E_i$	44.7 kJ/mol

The calculation code, which optimizes the capillary diffusivity expressed by eq (13), still has the parameters of potato as starting values (Datta, 2007):

**Table 26.** Starting parameters in optimization of capillary diffusivity

Name	Value
A	$10^{-9} \text{ m}^2/\text{s}$
B	2.8
C	2

The other parameters with dependencies by temperature and water concentration are literature correlations (Perry et al., 1998).

The development of the codes and the simulation runs have been carried out with a MS Windows workstation based on the Intel® Core™ i7-6700HQ processor with 2.60 GHz clock rate and 32 GB RAM.

#### 4.4 Simulation results

The simulation work has been started by taking as a reference the experimental test drying was considered under forced air circulation, that is conditions corresponding to values of air temperature, relative humidity and velocity as averaged over the whole duration of the test, i.e., 3 days. The effective diffusivity in eq. 12 was used.

The Figure 44 A and B are examples of the way the profile of water concentration can be graphically reported as a function of time through the length of the sample in both the configurations of the experimental test.

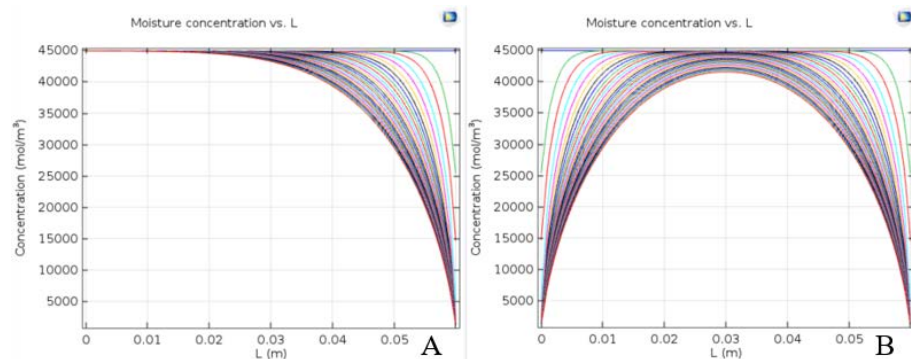


**Figure 44.** Water concentration ( $\text{mol/m}^3$ ) profile through the length of the sample  $L$  (m) parametrically in the drying day for test A (A) and test B (B)

The Figure 45A and B show the 3D color plot of the water concentration ( $\text{mol/m}^3$ ) in the specimen at the end of day 3 in both types of the experimental configuration.

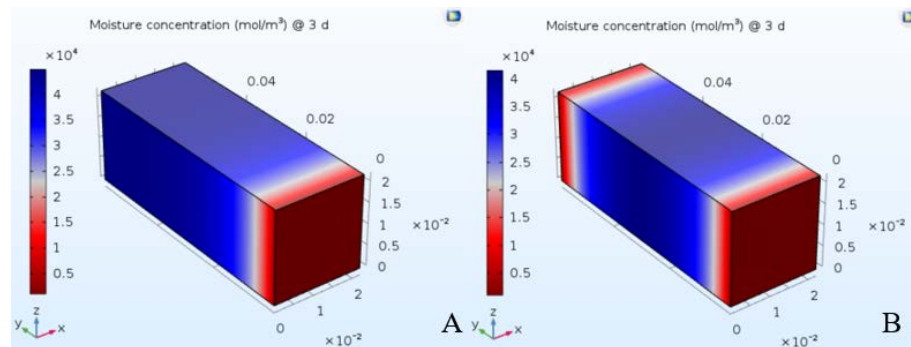


**Figure 45.** 3D plot of the water concentration ( $\text{mol/m}^3$ ) in the sample at day 3 for test A (A) and test B (B)

## 4.5 Comparison between predicted and experimental results

The comparison between predicted and experimental results takes place in two steps: the first one with experimental data with a “simple” literature expression of diffusivity such as eq (12) and the second one with an optimization code of the parameters that appear in the diffusivity eq. (8) and eq. (13), respectively.

### 4.5.1 Drying

Using the linear diffusivity formulation for swordfish eq. (12) (Zogzas, 2013), the goodness of the acquired experimental data was assessed.

There is a good agreement with experimental and simulated weight loss (Figure 46, Figure 47) for either type of the experimental configurations. In addition, the figures highlight the standard deviation in the acquired experimental data.

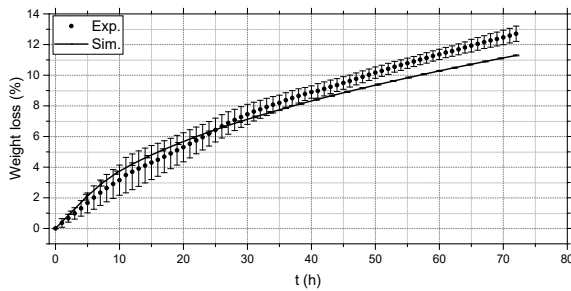


**Figure 46.** Comparison between experimental and predicted weight loss for one exchange surface experiment

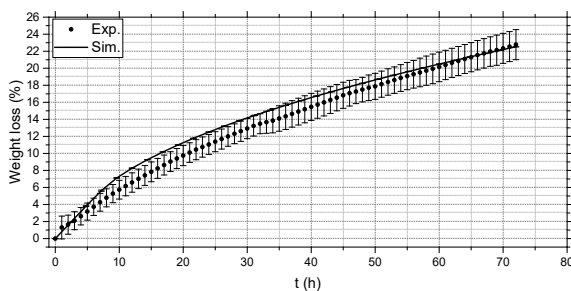


**Figure 47.** Comparison between experimental and predicted weight loss for two exchange surfaces experiment

Vice versa, when comparing the longitudinal profiles of moisture concentration (Figure 48A and B), the simulation is not that good because some simulation predictions are not close to the experimental data.

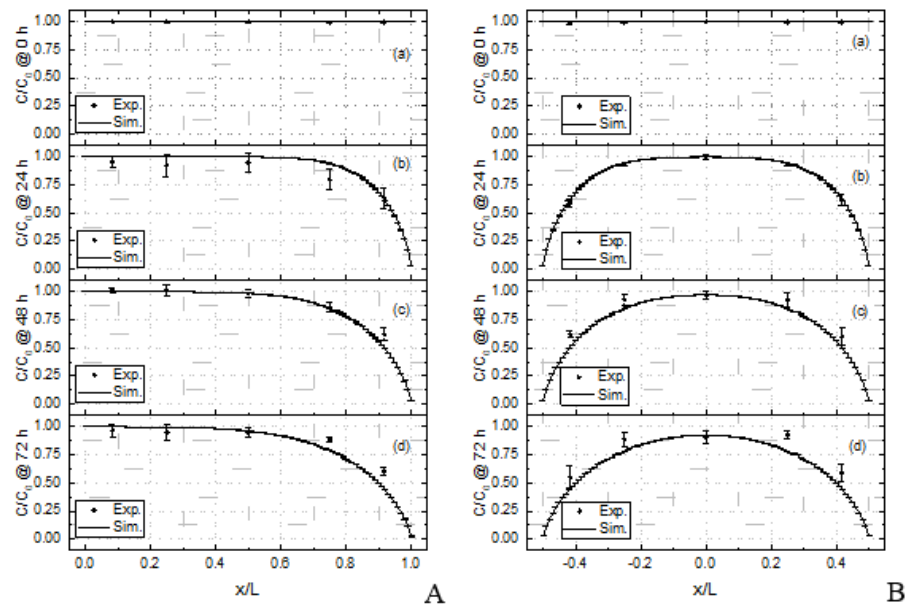


**Figure 48.** Comparison between experimental and predicted moisture concentration profile for one exchange surface experiment (A) and two exchange surfaces experiment (B)

#### 4.5.2 Optimization procedure for diffusivity parameter estimation

Then, the simulation runs were repeated by using the more realistic above-mentioned relationships for diffusivity eq. (8) and eq. (13), provided with the parameter values obtained by the optimization procedure.

First, the simulation with coupling modeling and optimization was started by adopting the effective diffusivity correlation in eq. (8) with the start parameters shown in Table 25.

During a repeated calculation cycle, the COMSOL code evaluates the mass transfer physics simulation results, compares them with the experimental selected data for optimization (weight loss and moisture concentration profiles in experimental test A), changes the current  $D_0$ ,  $D_i$ ,  $E_0$ ,  $E_i$  parameter values and starts a new simulation.

In this way, the software identifies a local minimum of the least squares errors function (selected as optimization algorithm) between predicted results and experimental data and provides the set of parameters corresponding to this minimum.

With the expression diffusivity eq. (8), the code provided the parameters set in Table 27.

**Table 27.** *Effective diffusivity parameters as optimization result*

Name	Value
$D_0$	$4.6217 \cdot 10^{-10} \text{ m}^2/\text{s}$
$D_i$	$3.6622 \cdot 10^{-9} \text{ m}^2/\text{s}$
$E_0$	69.319 kJ/mol
$E_i$	31.953 kJ/mol

The subsequent results were compared to the experimental data averaged among the experiments with one exchange surface (test A).

Both the simulation of the weight loss (Figure 49) and of the concentration profile (e.g. @ 48 h, Figure 50) are very close to the data obtained from the experiments.

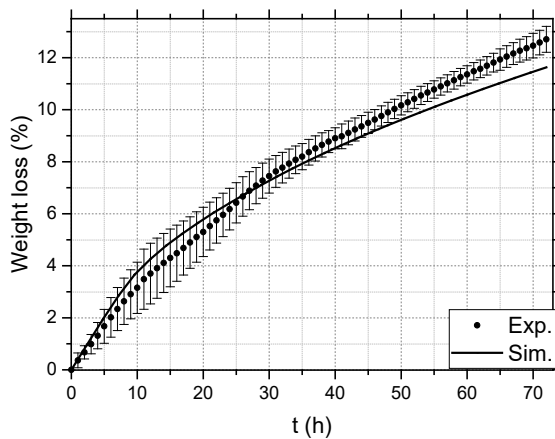


**Figure 49.** *Effective diffusivity simulation and experimental weight loss comparison for one surface experiment*

In order to have a further and independent validation of the mathematical model provided with the parameters obtained by the optimization procedure, a simulation was run under the conditions of the experiments with two exchange surfaces (test B). The weight loss predicted by such a simulation is reported in Figure 51 and compared to the experimental data, yielding a good closeness of the simulation results to the experimental ones.

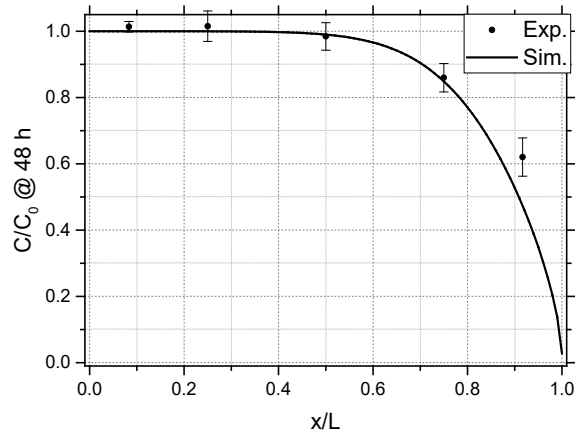


**Figure 50.** *Effective diffusivity simulation and experimental concentration profile comparison @ $t=48$  h for 1 surface experiment*

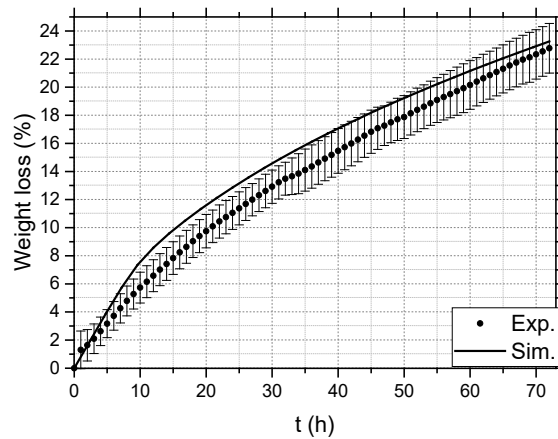


**Figure 51.** *Effective diffusivity simulation and experimental weight loss comparison for two exchange surfaces experiment*

Second, a similar job was done by running the simulation with the capillary diffusivity correlation eq. (13).

With the expression diffusivity eq. (13), the code provided the optimal parameter set:

**Table 28.** *Capillary diffusivity parameters as optimization result*

Name	Value
A	$1.4653 \cdot 10^{-9} \text{ m}^2/\text{s}$
B	2.3347
C	0.56064

The subsequent results were compared to the experimental data averaged among the experiments with one exchange surface (test A) (see Figure 52, Figure 53).

Then, with the parameters obtained by the optimization procedure, a simulation was run under the conditions of the experiments with two exchange surfaces (test B) (Figure 54).

The results are equally satisfactory.

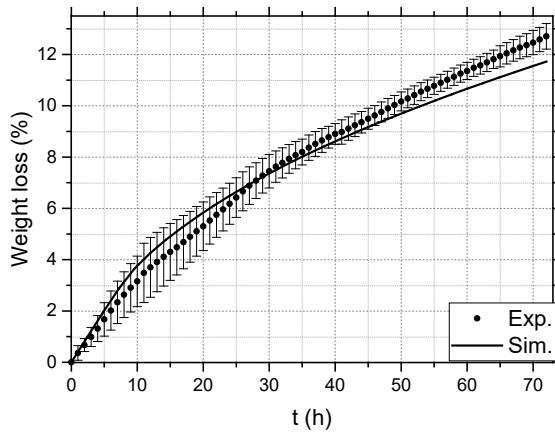


**Figure 52.** Capillary diffusivity simulation and experimental weight loss comparison for one surface experiment

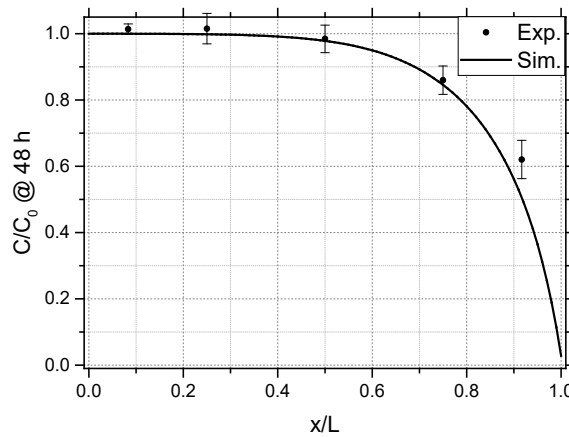


**Figure 53.** Capillary diffusivity simulation and experimental concentration profile comparison @t=48 h for one surface experiment

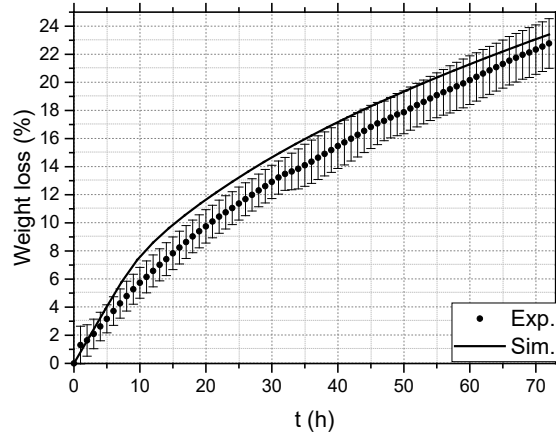


**Figure 54.** *Capillary diffusivity simulation and experimental weight loss comparison for two surface experiment*

#### 4.6 Conclusive remarks

By coupling the model simulation with porous media approach and the experimental data from the experimental apparatus, it is possible to simulate the drying process of a particular food component such as the minced lean meat (with difficult characteristics to be found in literature), which is the main component of the fresh sausage paste.

It was possible to optimize the coefficients that correlate the transport parameters to the operating conditions (e.g.,  $D=f(\text{local moisture content, Temperature})$ ) at typical temperatures of salami ripening and obtain specific correlations for the food under investigation.

# Conclusion and perspectives

This thesis deals with the development and the progressive improvement of a mathematical model of sausage drying during actual industrial ripening conditions.

The model simulations were compared with experimental data provided by literature and the industrial partner Dodaro SpA involved in the “Safemeat project”.

The simulation code allows understanding that a more realistic geometry is relevant on the computational load, but irrelevant on the prediction of the sausage weight loss. For this reason, a cylindrical shape can be used to implement a variable volume model simulation to realize a model closer to the reality. Another result was that the ripening process can be considered isothermal because the temperature transient occurs on a timescale that is negligible when compared to that characteristic of mass transfer.

Moreover, a new model, which considers the sausage as a heterogeneous material, e.g. separately made of lean meat and fat, using a porous medium approach was developed. The fat is considered as an inert matter dispersed in the meat matrix, while the lean meat is considered as a porous medium where the transport phenomena involved in the water movement take place to the outside of the matrix during the ripening process.

During the study, a lack of correlations for the water diffusion in the porous meat matrix has been highlighted (e.g.  $D=f(\text{moisture content})$ ). For this reason, an experimental apparatus and its procedure were realized to allow an evaluation of the dependence of the diffusivity from the local water content in the meat matrix during the drying process. The experimental apparatus allowed real-time monitoring of the weight and water concentration profiles that establish in the material under investigation.

By coupling the model simulation with porous media approach and the experimental data, it was possible to simulate the drying process of a particular material for which the internal water diffusion characteristics are unavailable or unrealistic in the literature.

Therefore, the method set up to evaluate the diffusion coefficient of a foodstuff matrix, coupled with the use of the mathematical model developed during this work, provides a more realistic simulation of the weight losses happening during the drying process and a deeper knowledge of the transport phenomena involved during this process.



# Bibliography

Baldini P., Castellani L., Diaferia C., Miccio M., Okasha F., 2001, Issues and steps in modeling salami drying, Proc. of ICheaP5, Florence, Italy, May 20-23, 879-884.

Baldini P., Diaferia C., Corbani P., Rossi A., Sarra P.G., Zacconi C., Vescovi M., 2006, I microrganismi nella produzione dei salumi tradizionali: aspetti igienici e tecnologici, *Ingegneria Alimentare*, 3, 8, 3-7.

Bertolini M., Ferretti G., Grassi A., Montanari R., "Ripening process design optimization for an ascending flow ripening chamber". *Journal of Food Engineering*, 77, 529–538, 2006.

Bessadok Jemai A., 2013, Characterizing The Drying Kinetics Of High Water Content Agro-Food Particles Exhibiting Non-Fickian Mass Transport. *Chemical Engineering Transaction*, 32

Cevoli, C., Fabbri, A., Tabanelli, G., Montanari, C., Gardini, F., Lanciotti, R., Guarnieri, A., 2014, Finite element model of salami ripening process and successive storage in package. *J. Food Eng.* 132, 14–20.

Costa-Corredor A., Pakowski Z., Lenczewski T., Gou P., 2010, Simulation of simultaneous water and salt diffusion in dry fermented sausages by the Stefan–Maxwell equation. *Journal of Food Engineering*, 97, 311–318.

Datta A.K., 2007, Porous media approaches to studying simultaneous heat and mass transfer in food processes. I: Problem formulations. *Journal of Food Engineering* 80, 80–95.

Datta A.K., 2007, Porous media approaches to studying simultaneous heat and mass transfer in food processes. II: Property data and representative results, *Journal of Food Engineering*, Vol 80, 96–110.

Da-Wen Sun et al., 2002, CFD predicting the effects of various parameters on core temperature and weight loss profiles of cooked meat during vacuum cooling. *Computers and Electronics in Agriculture* 34, 111–127.

De Rosa M., Diaferia C., Lanni A., Lo Iudice R., Magliano V., Miccio M., Pirone G., 2005, Bresaola from young buffalo: experimental production and steps towards mathematical modeling, *AIDIC Conference Series*, 7, 67-76

Diaferia C., Miccio M., Baldini P., Castellani L., De Rosa M.L., Fraganza M., Lanni A., 2011, Codice di simulazione e potenzialità predittive per la stagionatura di salumi tradizionali. *Industria Conserve*, ISSN: 0019-7483, anno LXXXV, n. 3, 161-173.

DRIP-Dry Sausages Ripening Improvement Project, 2000, Rapporto finale del progetto FAIR No. CT 96-1220.

Fabbri, A., Cevoli, C., 2015, 2D water transfer finite elements model of salami drying, based on real slice image and simplified geometry. *Journal of Food Engineering* 158, 73–79.

Fabbri, A., Cevoli, C., Silaghi, F.A., Guarnieri, A., 2011, Numerical simulation of physical system in agri-food engineering. *J. Agric. Eng.* 4, 1–7.

Ferrara M., Magistà D., Epifani F., Cervellieri S., Lippolis V., Gallo A., Perrone G., Susca A., 2016b, Study of gene expression and OTA production by *Penicillium nordicum* during a small-scale seasoning process of salami. *International Journal of Food Microbiology*, 227, 51–55.

Ferrara M., Magistà D., Lippolis V., Cervellieri S., Susca A., Perrone G., 2016a, Effect of *P. nordicum* contamination rates on ochratoxin A accumulation in dry cured salami. *Food Contr.*, 67, 235–239.

Feyissa A.H., Adler-Nissen J., Gernaey K.V., 2009, Model of Heat and Mass Transfer with Moving Boundary during Roasting of Meat in Convection-Oven. Excerpt from the Proceedings of the COMSOL Conference, Milan, Italy.

Grassi A. and Montanari R., 2005, Simulation of the thermodynamic patterns in an ascending flow ripening chamber. *Journal of Food Engineering*, 68, 113–123.

Grau, R., Andres, A. and Barat, J. M., 2014, Principles of Drying, in *Handbook of Fermented Meat and Poultry* (eds. F. Toldrá, Y. H. Hui, I. Astiasarán, J. G. Sebranek and R. Talon), John Wiley & Sons Ltd., Chichester, UK. DOI: 10.1002/9781118522653.ch5

Huff-Lonergan et al., 2005, Mechanisms of water-holding capacity of meat: The role of postmortem biochemical and structural changes. *Meat Science* 71, 194–204.

Imre L. and Kornyei T., 1990, Computer simulation of Salami drying. *International Journal for Numerical Methods in Engineering*, 30, 767-777.

Katz P., and Stinsky H., 1987, Determining optimum drying conditions for dry sausage products in ripening rooms. *Fleischwirtschaft*, 67(10), 1188.

Kottke V., Damm H., Fisher A., Leutz U., 1996, Engineering Aspects in Fermentation of Meat Products. *Meat Science*, 43, No. S, S243S255

Leistener L., 1987, in “Water Activity: Theory and Application to Food”, eds. L.B. Rockland, L.R. Beuchat, Marcel Dekker Inc., New York, Basilea, 295.

Letablier M. T., F. Nicolas, 1994, *Sci. Aliment.*, 14, 541.

Liicke F.K., 1994, Fermented meat products. *Food Research International* 27, 299-307.

Magistà D., Ferrara M., Del Nobile M.A., Gammariello D., Conte A., Perrone G., 2016, *Penicillium salamii* strain ITEM 15302: A new promising fungal starter for salami production. *International Journal of Food Microbiology*, 231, 33–41.

Okos M.R., G. Narsimhan, R.K. Singh, A.C. Weitnauer, 1992, in “Handbook of Food Engineering”, eds. D. R. Heldman, D. B. Lund, Marcel Dekker Inc., New York, Basilea, Hong Kong, 437.

Pearce et al., 2011, Water distribution and mobility in meat during the conversion of muscle to meat and ageing and the impacts on fresh meat quality attributes. *Meat Science* 89, 111–124.

Perry et al., 1998, *Chemical Engineers’ Handbook*, 7<sup>th</sup> Ed., McGraw-Hill, New York (USA).

Pirone G., Diaferia C., Iaccarino T., Madonia G., Demarco V., Pruiti V., Ripening techniques and microbiological characteristics of Nebrodi salame. Proceedings of 6th International Symposium on the Mediterranean Pig, Capo d’Orlando (ME), 11-13 ottobre 2007.

Rossen J.L., Hayakawa K., 1977, Simultaneous Heat and Moisture Transfer in Dehydrated Food: A Review of Theoretical Model. *AIChESym Series*, 73, 71.

SAFEMEAT, 2013, <http://www.dodaro.com/safemeat/index.html> (in Italian)

Salomie I., Tudor Cioara, Ionut Anghel, Mihaela, Dinsoreanu, Tudor Ioan Salomie, 2007, Workflow Models Enhanced with Process Algebra Verification for Industrial Business Processes, Proc. of the 11th WSEAS International Conference on COMPUTERS, Agios Nikolaos, Crete Island, Greece, July 26-28.

Saravacos G.D., 2001, *Transport Properties of Foods*, 106, 200, 201.

Spotti, E., Berni, E., Cacchioli, C., 2008, Characteristics and applications of molds, in: Toldrà, F. (Ed.), *Meat Biotechnology*. Springer Science + Business Media LLC, New York, 181–195.

Toldrà F., 2010, *Handbook of Meat Processing*, 385.

Toldrà F., Hui Y. H., Astiasarán Iciar, Sebranek Joseph G., Talon Règine, 2014, *Handbook of Fermented Meat and Poultry*, 2nd Edition, John Wiley & Sons Ltd., Chichester, UK. DOI: 10.1002/9781118522653

Various authors, 2013, Rapporto Tecnico su Stato Avanzamento n.4. 15.04–14.10.2013 PON SAFEMEAT.

Zambonelli C., Luigi Grazia, Fausto Papa, Patrizia Romano, Giovanna Suzzi, 1992, *Microbiologia dei salumi*, Edagricole - New Business Media, pp.170–173.

Zeuthen, P., 2007, A Historical Perspective of Meat Fermentation, in *Handbook of Fermented Meat and Poultry* (ed. F. Toldrà), Blackwell Publishing Ltd, Oxford, UK. DOI: 10.1002/9780470376430.ch1

Zogzas N.P., Z.B. Maroulis & D. Marinos-Kouris, 2013, Moisture Diffusivity Data Compilation in Foodstuffs. *Drying Technology: An International Journal*, 14:10, 2225-2253.



# APPENDIX A

## Arduino programming

```
#include <HX711.h>
#include <DHT.h>
/*
  pin 2 -> CLK
  3 -> DAT
  5V -> VCC
  GND -> GND
  The HX711 board can be powered from 2.7V to 5V so the Arduino 5V
  power should be fine.
  */
#define calibration_factor -12307//This value is obtained using the
SparkFun_HX711_Calibration sketch
#define DOUT 3
#define CLK 2
#define DHTPIN 7
#define DHTTYPE DHT22
HX711 scale(DOUT, CLK);
DHT dht(DHTPIN, DHTTYPE);
int MatriceSold1=0;
int MatriceSold2=0;
int MatriceSold3=0;
int MatriceSold4=0;
int MatriceSold5=0;
//Excel
int x = 0;
int row = 0;
const int analogInPin = A0;
int sensorValue = 0;
int outputValue = 0;
void setup() {
  Serial.begin(9600);
  dht.begin();
  //Serial.println("HX711 scale demo");
  scale.set_scale(calibration_factor); //This value is obtained by using the
SparkFun_HX711_Calibration sketch
```

```

    scale.tare();          //Assuming there is no weight on the scale at start up,
reset the scale to 0
    Serial.println("READINGS:");
    //Excel
    Serial.println("CLEARDATA");
    Serial.println("LABEL,Time,Weight [g],Air Humidity [%],Air
Temperature [*C],Sample Moisture 1 [mV],Sample Moisture 2 [mV],Sample
Moisture 3 [mV],Sample Moisture 4 [mV],Sample Moisture 5 [mV]");
}
void loop() {
    Serial.println("-----");
    Serial.print("Weight: ");
    Serial.print(scale.get_units(), 3); //scale.get_units() returns a float
    Serial.println(" g"); //You can change this to kg but you'll need to refactor
the calibration_factor
    //DHT22
    float h = dht.readHumidity();
    // Read temperature as Celsius (the default)
    float t = dht.readTemperature();
    Serial.print("Air Humidity: ");
    Serial.print(h);
    Serial.println(" %\t");
    Serial.print("Air Temperature: ");
    Serial.print(t);
    Serial.println(" *C ");
    Serial.println("(Inside)SM1->SM2->SM3->SM4->SM5(Outside)");
    //moisture sensor
    // read the input on analog pin 0:-----
    int MatriceSold1 = analogRead(A0);
    Serial.print("Sample Moisture 1: ");
    Serial.print(MatriceSold1);
    Serial.println(" mV");
    delay(0000); // delay in between reads for stability----
    int MatriceSold2 = analogRead(A1);
    Serial.print("Sample Moisture 2: ");
    Serial.print(MatriceSold2);
    Serial.println(" mV");
    delay(0000);
    int MatriceSold3 = analogRead(A2);
    Serial.print("Sample Moisture 3: ");
    Serial.print(MatriceSold3);
    Serial.println(" mV");
    delay(0000);
    int MatriceSold4 = analogRead(A3);

```

---

```
Serial.print("Sample Moisture 4: ");
Serial.print(MatriceSold4);
Serial.println(" mV");
delay(0000);
int MatriceSold5 = analogRead(A4);
Serial.print("Sample Moisture 5: ");
Serial.print(MatriceSold5);
Serial.println(" mV");
delay(0000);
//Excel
Serial.print("DATA,TIME,");
Serial.print(scale.get_units(), 3); Serial.print(",");
Serial.print(h); Serial.print(",");
Serial.print(t); Serial.print(",");
Serial.print(MatriceSold1); Serial.print(",");
Serial.print(MatriceSold2); Serial.print(",");
Serial.print(MatriceSold3); Serial.print(",");
Serial.print(MatriceSold4); Serial.print(",");
Serial.print(MatriceSold5); Serial.print(",");
row++;
x++;
if (row > 1000000000)
{
row=0;
Serial.println("ROW,SET,2");
}
delay(300000);
}
```